applied sciences

MDPI

Article

Analytical Protocol for the Scientific Investigation of Black Crusts on the Exterior Finish of the West Enclosure Wall of Golia Monastery (Iași, Romania): A Case Study on Urban Pollution Impact

Vasile Pelin [1,2], Viorica Vasilache [3], Silvia Garofalide [1,2], Ioan-Andrei Dascalu [4], Ovidiu Chiscan [5], Bobi Apavaloaei [6], Silviu Gurlui [1,2,*] and Ion Sandu [3,7,8,9,*]

1 Laboratory of Applied Meteorology and Climatology, Research Center with Integrated Techniques for Atmospheric Aerosol Investigation in Romania—RECENT AIR Department of Exact Sciences and Natural Sciences, The Institute of Interdisciplinary Research, Alexandru Ioan Cuza University of Iași, A Building, Physics, 11 Carol I Bld., 700506 Iași, Romania; vasilepelin@yahoo.com (V.P.); silvia.garofalide90@gmail.com (S.G.)
2 Atmosphere Optics, Spectroscopy and Laser Laboratory LOASL, Faculty of Physics, Alexandru Ioan Cuza University of Iași, 11 Carol I Bld., 700506 Iași, Romania
3 ARHEOINVEST Center, Department of Exact Sciences and Natural Sciences, The Institute for Interdisciplinary Research, Alexandru Ioan Cuza University of Iaşi, Carol I Boulevard, no. 11, 700506 Iași, Romania; viorica_18v@yahoo.com
4 Center of Advanced Research in Bionanoconjugates and Biopolymers, Petru Poni Institute of Macromolecular Chemistry, 41A Grigore Ghica Voda Alley, 700487 Iași, Romania; idascalu@icmpp.ro
5 Faculty of Physics, Alexandru Ioan Cuza University of Iași, 11 Carol I Bld., 700506 Iași, Romania; ovidiu.chiscan@uaic.ro
6 Institute of Archaeology, Romanian Academy, Iași Branch, 6 Codrescu St., Pavilion H, 700479 Iași, Romania; bobiapv@yahoo.com
7 Academy of Romanian Scientists AOSR, 54 Splaiul Independentei St., Sector 5, 050094 Bucharest, Romania
8 National Institute for Research and Development in Environmental Protection, 294 Splaiul Independentei St., Sector 6, 060031 Bucharest, Romania
9 Romanian Inventors Forum, Sf. Petru Movila St., L11, 3-3, 700089 Iași, Romania
* Correspondence: sgurlui@uaic.ro (S.G.); sandu_i03@yahoo.com (I.S.)

Featured Application

The analytical protocol presented in this study provides a practical diagnostic framework for identifying and characterizing black crusts on historic lime mortars exposed to urban pollution. In the local conservation context (Iași and comparable Romanian historic cities), it supports minimally invasive, evidence-based intervention planning by linking rapid screening and cross-validated laboratory markers to treatment selection and post-intervention monitoring.

Abstract

Black crusts are multilayered alteration products that develop on historic masonry exposed to urban pollution. This study investigates the west enclosure wall of the XVIIth-century Golia Monastery in Iași, Romania—located along a busy traffic corridor—and presents multi-analytical results on two lime-based mortar fragments exhibiting well-developed blackened surface layers. Both the exposed (blackened) finishes and protected verso areas were analyzed using portable X-ray fluorescence (pXRF), scanning electron microscopy with energy-dispersive X-ray analysis (SEM–EDX), micro-FTIR spectroscopy, X-ray diffraction (XRD), CIE Lab colorimetry and optical microscopy (OM). The data reveal gypsum-rich surface layers enriched in traffic-derived particles, including metal oxides and soot, with marked contrasts relative to the minimally altered verso. Handheld XRF and SEM–EDX indicate elevated sulfur and associated traffic-related elements within porous gypsum

Check for updates

Academic Editor: Roberto Zivieri

Received: 15 December 2025
Revised: 15 February 2026
Accepted: 16 February 2026
Published: 20 February 2026

Copyright: © 2026 by the authors. Licensee MDPI, Basel, Switzerland. This article is an open access article distributed under the terms and conditions of the Creative Commons Attribution (CC BY) license.

matrices, while FTIR and XRD consistently identify calcium sulfate as the dominant secondary phase. Colorimetric measurements additionally document pronounced lightness loss and visible darkening on exposed surfaces. These results demonstrate the onset of directional sulfation and black crust formation on mortars under urban pollution pressure and establish an integrated analytical protocol for diagnosing black crusts on historic lime mortars in urban heritage settings.

Keywords: black crusts; historic lime mortars; directional sulfation; portable X-ray fluorescence (pXRF); CIE Lab colorimetry; urban air pollution; architectural heritage conservation

1. Introduction

Stone-built architectural heritage is highly vulnerable to atmospheric pollution, and black crusts formed on carbonate substrates are among the most characteristic expressions of this interaction. These crusts typically consist of multilayered gypsum accumulations incorporating carbonaceous particles, metal-rich aerosols and resuspended road dust; they induce visible darkening, weaken the crust–substrate interface and may function as passive archives of urban atmospheric composition over decadal timescales [1–4]. This dual role—as both a deterioration feature and a geochemical recorder—has been widely exploited to reconstruct past sulfur loads and to evaluate the effects of air-quality regulations on monument surfaces. Recent studies further show that black crusts capture evolving particulate mixtures in present-day cities, including traffic-derived metal oxides, secondary nitrates and anthropogenic sulfates [1,3].

The development and persistence of black crusts are controlled by the composition of air pollutants, substrate mineralogy and pore structure, surface micro-topography and local microclimate. These factors govern whether crusts thicken in sheltered recesses, are periodically washed by runoff, or are reworked by splash water and wind-blown particles [1,5,6]. Within the broader research on historic mortars—emphasizing their conservation relevance, bonding performance, and distinctive hygric/physico-chemical behavior [7–9]—the specific issue of pollution-driven black-crust development on exterior mortar finishes (including restoration mortars) remains a priority, even where crust occurrence is still at an early stage and not yet visually advanced. Mortars, with higher porosity and binder heterogeneity, may respond differently to pollutant inputs and moisture regimes, yet their alteration pathways under urban exposure remain insufficiently documented.

Multi-analytical approaches are now standard tools for diagnosing black crusts and surface soiling, combining portable X-ray fluorescence (pXRF), vibrational spectroscopy and microscopy to relate elemental distributions, mineralogical phases and chromatic shifts [1,5,10–12]. CIE Lab colorimetry provides quantitative assessment of soiling intensity, perceptual color thresholds and the effects of cleaning treatments on stone and mortar surfaces [5,11,12]. When integrated with X-ray diffraction (XRD), Fourier-transform infrared (FTIR) spectroscopy and scanning electron microscopy with energy-dispersive X-ray spectroscopy (SEM–EDX), such protocols allow reconstruction of the coupled chemical, mineralogical and microstructural evolution of crusts and their substrates in complex urban atmospheres.

The historic Golia Monastery in Iași (north-eastern Romania) provides a particularly suitable case study. The west enclosure wall and its buttresses directly border a heavily trafficked urban street and receive combined inputs from local vehicle emissions, resuspended dust and regionally transported "urban exotic pollution" [6]. A recent conservation state assessment has documented widespread mortar deterioration, localized stone scaling

and emerging black crusts along the enclosure wall, underscoring the need for spatially resolved diagnostic work [13]. Complementary pXRF screening of limestone blocks on the western buttress has shown strong enrichment in sulfur, chlorine, heavy metals and other non-lithogenic elements in crusts relative to underlying stone, confirming the sensitivity of this façade to present-day pollution episodes [14]. In contrast, the mortars of the same enclosure wall and its buttresses—particularly the restoration mortars applied during the 2008–2010 conservation campaign—have not yet been analyzed in detail, despite visible chromatic and textural contrasts between exposed and sheltered surfaces.

The multi-analytical diagnostic strategy adopted here follows recent developments in conservation science, which emphasize integrated methodologies, interdisciplinary interpretation and the harmonization of terminology for heritage materials [15–17]. These approaches, together with recent contributions on innovative conservation materials and advanced intervention procedures [18,19], provide a conceptual framework for assessing the behavior of lime-based mortars under urban pollution exposure.

Against this background, the present study investigates two representative restoration mortar samples taken from one western enclosure buttress of Golia Monastery, aiming to capture the early stages (~15–17 years) of pollution-driven alteration in exposed joints. The multi-technique results presented below show that alteration is already significant within the outer millimeters, that it is strongly directional with respect to wall orientation and prevailing traffic flows, and that these geochemical and chromatic gradients have direct implications for conservation zoning and maintenance strategies along the Golia enclosure wall.

2. Materials and Methods

2.1. Site Description and Sampling

The analytical protocol adopted in the present study combines site-specific sampling with a series of complementary techniques applied to a limited number of representative mortar fragments. The investigation focuses on a western buttress of the enclosure wall of Golia Monastery, located along George Enescu Street in the center of Iași, Romania (47°09′54.0″ N, 27°35′17.9″ E), directly facing a busy urban traffic corridor (Figure 1a–c). Two small lime-based mortar fragments detached from deteriorated and degraded joints on this buttress were collected and labeled N (dark, black-crusted mortar) and A (light-colored mortar). For each sample, three distinct surface types were investigated: (i) the exposed faces bearing black crusts and directly facing the street (Nf, Af) (Figure 1d), (ii) the protected verso surfaces oriented towards the interior of the wall (Nv, Av) (Figure 1e), and (iii) freshly exposed fracture surfaces of the same fragments (N and A), revealing the inner mortar core and used as reference zones (Nc, Ac) (Figure 1f). For objective reasons related to the flattened geometry of the mortar fragments and technical constraints on positioning or exposing the inner-core surfaces within the available analytical instruments, the Nc and Ac inner-core areas were only investigated by CIE Lab colorimetry and optical microscopy and were not subjected to pXRF, SEM–EDX, FTIR or XRD analysis. This sampling method allows a direct comparison between pollution-exposed and sheltered micro-environments within the same joints while still maintaining a non-destructive or minimally invasive approach to the historic material.

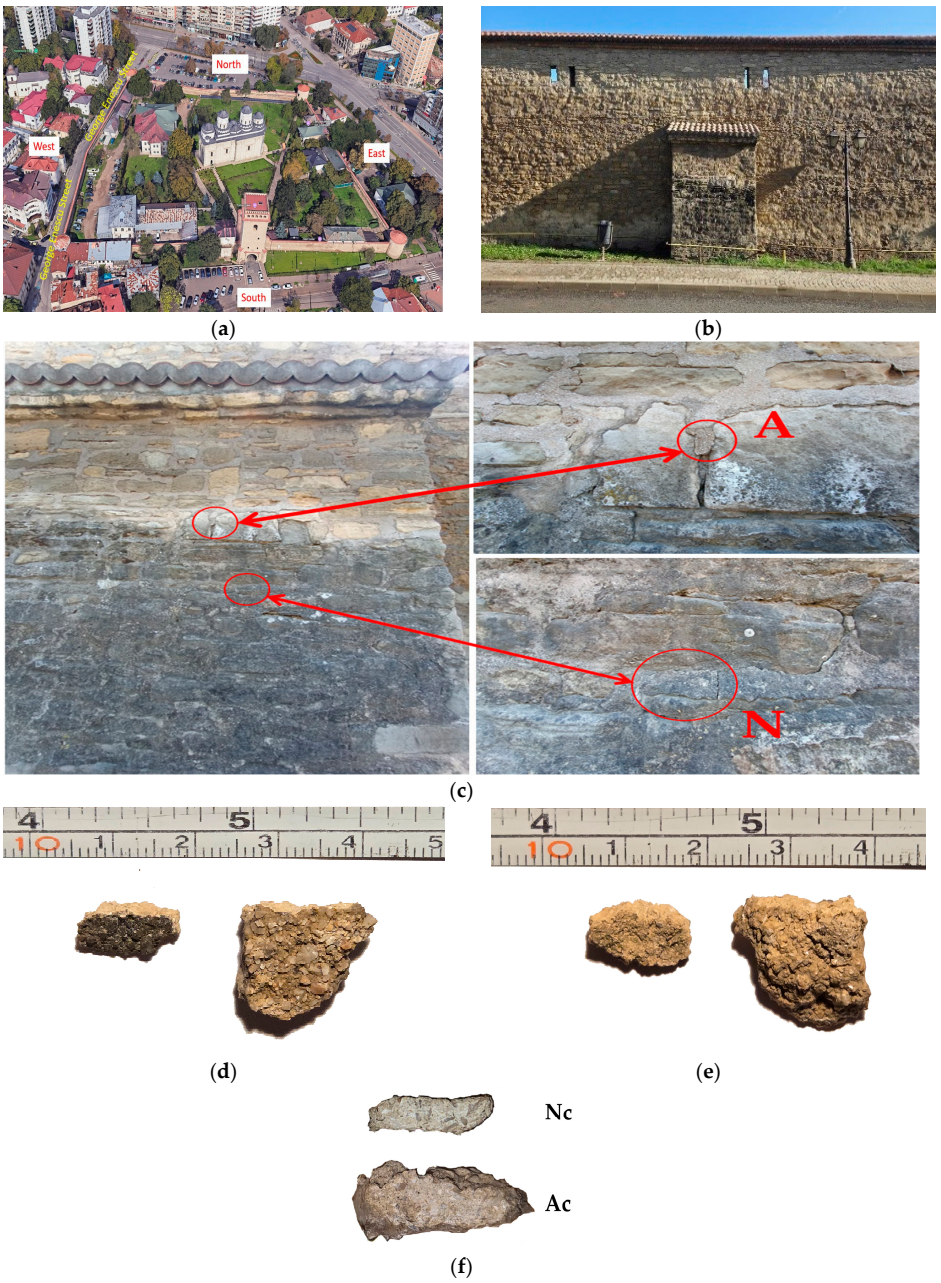


Figure 1. Site context of the investigated wall section at Golia Monastery (Iași, Romania): (**a**) aerial view of the Golia Monastery ensemble, showing the orientation of the west enclosure wall parallel to George Enescu Street and the position of the cardinal directions (N–S–E–W) (source: Google Earth) [14]; (**b**) street-level view of the western wall and its buttresses, with the roadway axis located ≈4.90 m from the buttress base (47°09′54.0″ N, 27°35′17.9″ E); (**c**) sampling area for the two collected mortar fragments: light-colored mortar (sample A) and blackened mortar (sample N); (**d**) exposed faces of the mortar fragments, directly facing the exterior environment and analogous to the buttress front: left—Nf, right—Af; (**e**) verso surfaces (Nv, Av) corresponding to the backs of the same samples, indirectly exposed to the environment and facing to the interior of the wall; (**f**) freshly exposed fracture surfaces of the same fragments (N and A), revealing the inner mortar core; designated as reference zones (Nc, Ac).

2.2. Analytical Techniques

The two samples were investigated by a multi-technique workflow: portable X-ray fluorescence (pXRF), scanning electron microscopy with energy-dispersive X-ray spectroscopy

(SEM–EDX), Fourier transform infrared spectroscopy (FTIR), X-ray diffraction (XRD), CIE Lab colorimetry and optical microscopy (OM).

2.2.1. Portable X-Ray Fluorescence (pXRF)

Portable X-ray fluorescence measurements were performed with a Bruker S1 TITAN handheld spectrometer (Bruker Nano, Berlin, Germany) equipped with a rhodium-anode X-ray tube (up to 50 kV, 4 W maximum power) and a 20 mm^2 silicon drift detector (SDD) with a typical energy resolution of <145 eV at Mn Kα. The instrument was operated under the GeoExploration application using the factory Oxide three-phase calibration suitable for silicate and carbonate matrices. All analyses were carried out in the laboratory using the dedicated Bruker benchtop stand with safety interlocks: the spectrometer was fixed in the stand, and each surface of the mortar sample was placed in direct contact with the examination window inside the closed sample compartment, ensuring a constant geometry and shielding from ambient laboratory conditions.

Each measurement consisted of a three-beam sequence at 15, 30 and 50 kV (tube currents 8.75, 11.8 and 17 μA, respectively), with 30 s live time per beam (total acquisition time 90 s). An 8 mm collimator was used throughout and the instrument was run in "Blank" filter mode. Elemental concentrations for major and trace elements relevant to crust formation (from Mg to Pb) were calculated and reported as weight percent (wt.%) using the manufacturer's fundamental-parameters algorithm. Measurements were non-destructive. Instrument performance was routinely checked against the certified Bruker reference sample supplied with the device.

2.2.2. Scanning Electron Microscopy with Energy-Dispersive X-Ray Spectroscopy (SEM–EDX)

SEM–EDX was performed using a VEGA II LSH scanning electron microscope (TESCAN, Brno, Czech Republic) equipped with a tungsten filament electron gun, coupled to a QUANTAX QX2 EDX system (Bruker/Roentec, Berlin, Germany). The SEM provides a nominal resolution of 3 nm at 30 kV, with a magnification range from 30× to 1,000,000×, accelerating voltages between 200 V and 30 kV, and scan times from 200 ns to 10 ms per pixel under high-vacuum conditions (working pressure < 1×10^{-2} Pa). Secondary electron (SE) and backscattered electron (BSE) signals were used to document surface morphology, microcracks and textural relationships in the mortar and crusts.

Elemental microanalysis was carried out with the third-generation X-Flash QUANTAX QX2 EDX detector and provides faster acquisition compared with conventional Si (Li) detectors. Small fragments were analyzed as received, without polishing or embedding, in order to preserve their original surfaces; the procedure is therefore effectively non-destructive at the sample scale.

2.2.3. Fourier Transform Infrared Spectroscopy (FTIR)

FTIR measurements were carried out using a TENSOR 27 FTIR spectrometer (Bruker Optics, Ettlingen, Germany) equipped with a standard DLaTGS detector, covering the 7500–370 cm^{-1} spectral range at room temperature, and providing a typical spectral resolution of 4 cm^{-1} (down to 1 cm^{-1} when required). The instrument incorporates a He–Ne reference laser (633 nm, 1 mW) and a ROCKSOLID interferometer alignment system and is fully controlled by the OPUS software v6.5 Build 20070524 (Bruker Optics, Ettlingen, Germany). For micro-analytical work, the TENSOR 27 was coupled to a HYPERION 1000 FTIR microscope (Bruker Optics, Ettlingen, Germany), allowing non-destructive measurements on small solid fragments in reflection mode. The microscope is fitted with a liquid-nitrogen-cooled MCT detector (operating at −196 °C), an objective with 15× magnification and an adjustable sampling area optimized around 250 μm in diameter, with a minimum spot size of approximately 20 μm. Spectra were acquired in the mid-IR region relevant for

mineral and salt phases. Small samples were analyzed without embedding or mechanical preparation, ensuring that the investigation remained non-destructive and that the surface stratigraphy was preserved.

2.2.4. X-Ray Diffraction (XRD)

X-ray diffraction (XRD) analysis was performed with a Rigaku SmartLab diffractometer (Tokyo, Japan) equipped with a Cu anode (X-ray wavelength of 1.5406 Å) operating at 45 kV and 200 mA. Approximately 2 mm in depth of each sample face was collected and ground into a powder prior to the analysis. Sample phase composition was identified using Match! software v3.15i [20] and the Crystallography Open Database. The identified crystallographic information files of quartz SiO_2 (COD entry no. 96-901-0147), calcite $CaCO_3$ (COD entry no. 96-900-9669) and calcium sulfate dihydrate $CaSO_4 \cdot 2H_2O$ (COD entry no. 96-500-0040) were used to calculate the theoretical diffraction patterns and compare them to that of the measured samples.

2.2.5. Colorimetric Measurements (CIE Lab)

Colorimetric measurements were performed with a portable precision colorimeter NR10QC (3Nh Technology Co., Ltd., Shenzhen, China). The instrument operates with an 8/d illuminating/viewing geometry (8° illumination, diffuse viewing), a 4 mm circular measuring aperture and a silicon photoelectric diode detector. It uses an internal D65 LED light source and reports color coordinates in several standard spaces, including CIE Lab, and color-differences (ΔE_{00}) between pairs of surfaces were calculated with the standard CIE DE2000 equation [21,22]:

$$\Delta E_{00} = \sqrt{\left(\frac{\Delta L'}{k_L S_L}\right)^2 + \left(\frac{\Delta C'}{k_C S_C}\right)^2 + \left(\frac{\Delta H'}{k_H S_H}\right)^2 + R_T \left(\frac{\Delta C'}{k_C S_C}\right)\left(\frac{\Delta H'}{k_H S_H}\right)}$$

CIE Lab measurements were carried out non-invasively by gently placing the measuring aperture in direct contact with the mortar surfaces without any mechanical preparation, coating or sampling.

2.2.6. Optical Microscopy (OM)

OM observations were carried out using a reflected-light microscope, Zeiss Axio Imager A1m (Carl Zeiss, Microscopy, Jena, Germany), equipped with an Axiocam digital camera (Carl Zeiss Microscopy, Jena, Germany) and dedicated Zeiss imaging software AxioVs v4.7.1.0 (Carl Zeiss Imaging Solutions, München, Germany). The instrument was operated in episcopic bright-field (Epi-BF) mode, which is suitable for the examination of opaque building materials and surface coatings. Small mortar samples were mounted and analyzed as received in order to preserve the original surface morphology; the procedure is therefore effectively non-destructive at the sample scale. Overview images were acquired mainly with a 5× objective (5×_3_Epi_BF setting), allowing the roughness and chromatic heterogeneity of the investigated surfaces to be documented.

Each mortar surface (Nf, Nv, Af, Av, Nc, Ac) was documented through at least two micrographs taken at slightly different focal planes to capture the roughness of the surfaces or black crust.

3. Results

3.1. pXRF Results

Portable X-ray fluorescence (pXRF) analyses were performed on the four surfaces of the two mortar fragments: Nf, Nv, Af and Av. For each of the investigated surfaces Nf and Nv, three pXRF measurement points (spots) were selected, and each spot was

measured in three replicates. For the Af and Av surfaces, which have slightly larger areas, five measurement points (spots) were selected, with each spot likewise measured in three replicates. In total, this resulted in 48 individual measurements, which are reported in Table S1. This table includes both mean values and standard deviations. The pXRF analyses of the Nf, Nv, Af, and Av surfaces of the two mortar fragments reveal compositional variations correlated with exposure conditions and crust development (Table 1), in agreement with the relevant literature [23–25].

Table 1. Mean ± SD pXRF composition of the four analyzed surfaces.

Surface	Oxide/Element												
	SiO_2	Al_2O_3	Ca	S	S Ca Ratio [1]	SiO_2 Ca Ratio [1]	SiO_2 Al_2O_3 Ratio [1]	Fe	Ti	Zn	Pb	P	Cl
Nf	48.81 ± 0.22	4.43 ± 0.02	12.39 ± 0.53	0.58 ± 0.06	0.050	3.94	11.01	1.67 ± 0.17	0.15 ± 0.01	0.03 ± 0.00	0.00	0.11 ± 0.01	-
Nv	26.66 ± 2.67	6.43 ± 1.07	25.55 ± 3.87	0.29 ± 0.03	0.010	1.05	4.18	1.95 ± 0.41	0.15 ± 0.04	0.01 ± 0.00	0.01 ± 0.00	0.11 ± 0.02	0.10 ± 0.05
Af	25.25 ± 5.09	2.10 ± 0.53	23.89 ± 4.31	0.25 ± 0.08	0.010	1.06	12.25	0.68 ± 0.24	0.02 ± 0.01	0.01 ± 0.00	0.00	0.05 ± 0.01	0.20 ± 0.18
Av	25.82 ± 3.39	4.93 ± 0.90	21.03 ± 1.88	0.57 ± 0.35	0.030	1.24	5.36	1.40 ± 0.25	0.09 ± 0.02	0.02 ± 0.01	0.01 ± 0.00	0.11 ± 0.01	0.08 ± 0.03

[1] Calculated as the ratio between mean concentrations obtained from pXRF data.

All surfaces are characterized by a calcareous (lime-based) siliceous matrix with variable Ca and SiO_2 proportions but with broadly consistent lithogenic elements such as Fe and Ti. This confirms that all measurements refer to the same mortar system, sampled at different depths and exposure states.

Technical Note on pXRF Sensitivity

Handheld pXRF instruments have reduced sensitivity to light elements such as Mg, Al, Si, P and S due to the low fluorescence yield and the strong absorption of low-energy X-rays by air and detector windows [26]. As a result, phosphate signals close to the detection limit should be interpreted with caution, since they may reflect instrument limitations rather than true chemical absence or presence in the material.

3.2. SEM–EDX Characterization

Scanning electron microscopy coupled with energy-dispersive X-ray spectroscopy (SEM–EDX) was employed to investigate the microstructural and elemental signatures associated with crust development, surface alteration and mortar preservation. SEM–EDX provides high-resolution imaging of surface textures (backscattered electrons—BSE and secondary electrons—S) (Figures 2–5) and quantitative elemental composition at the microscale (Table 2).

Table 2. Elemental composition (wt.%) obtained by EDX on the four investigated surfaces. (Nf, Nv, Af, Av, respectively zones 1 and 2).

Investigated Area		Element (wt.%)												
		O	Si	Ca	C	Al	Fe	Mg	Na	K	S	Cl	P	Ti
Nf	zone 1	57.26	21.00	5.21	4.86	4.17	2.34	1.55	1.48	1.48	0.37	0.28	–	–
	zone 2	53.52	26.72	4.87	4.31	3.23	2.30	1.3	1.26	1.52	0.60	0.39	–	–
Nv	zone 1	42.64	17.56	24.92	0.99	4.83	2.81	1.53	0.70	3.07	0.37	–	0.29	0.30
	zone 2	40.68	15.76	28.10	0.71	4.88	3.32	1.51	0.84	3.01	0.43	–	0.38	0.39
Af	zone 1	44.71	20.65	25.13	0.07	2.09	2.38	1.67	0.58	2.41	0.23	0.09	–	–
	zone 2	44.13	18.36	28.57	0.15	1.79	2.39	1.25	0.60	2.36	0.30	0.08	–	–
Av	zone 1	50.22	27.34	11.75	1.50	3.36	1.69	1.00	0.72	1.91	0.53	–	–	–
	zone 2	59.77	8.95	20.67	1.29	2.71	2.41	1.15	0.52	2.38	0.16	–	–	–

Notes: the symbol "–" indicates elements below detection or not quantified.

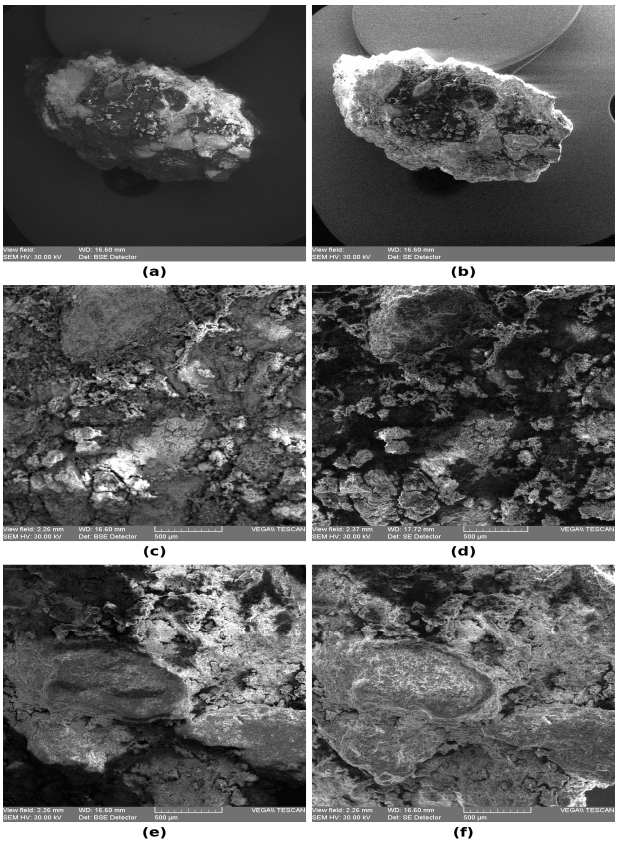


Figure 2. SEM images (BSE and SE) of sample Nf at two magnification levels: (**a**,**b**) whole-sample SEM imaging (BSE/SE), (**c**,**d**) microstructural detail in zone 1 (BSE/SE), (**e**,**f**) microstructural detail in zone 2 (BSE/SE).

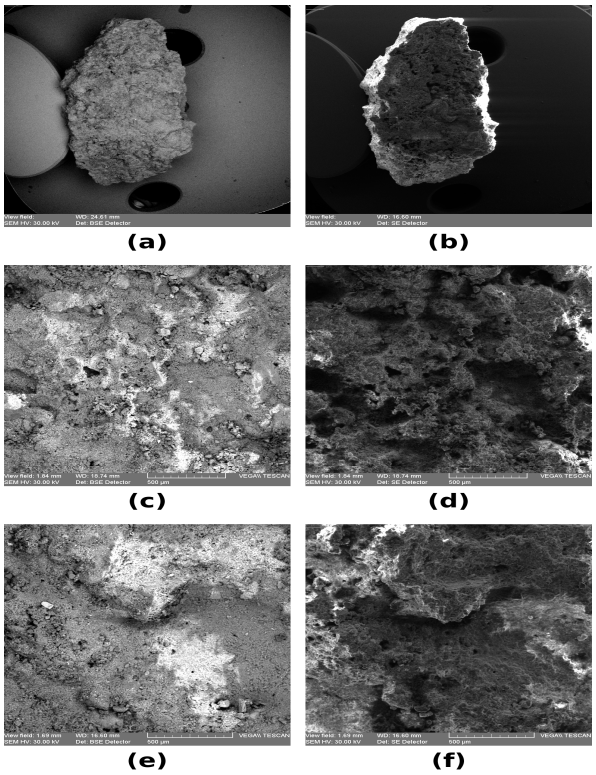


Figure 3. SEM images (BSE and SE) of sample Nv at two magnification levels: (**a**,**b**) whole-sample SEM imaging (BSE/SE), (**c**,**d**) microstructural detail in zone 1 (BSE/SE), (**e**,**f**) microstructural detail in zone 2 (BSE/SE).

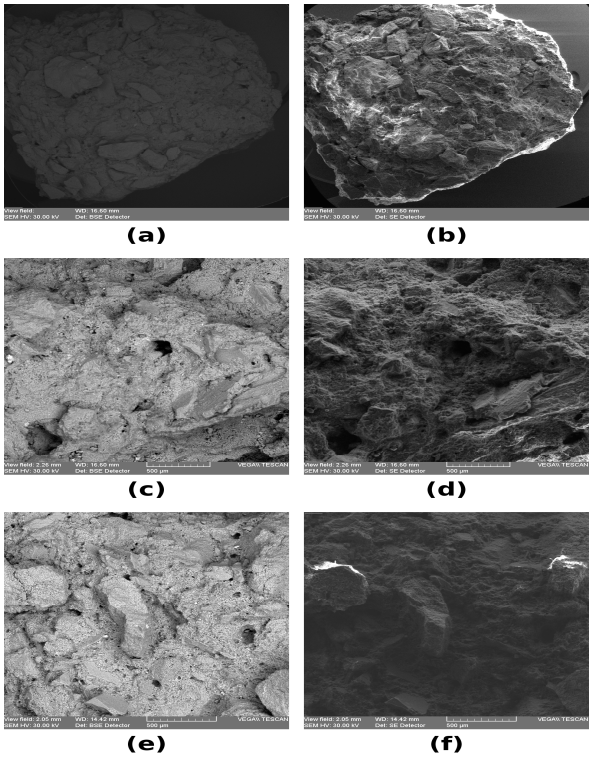


Figure 4. SEM images (BSE and SE) of sample Af at two magnification levels: (**a**,**b**) whole-sample SEM imaging (BSE/SE), (**c**,**d**) microstructural detail in zone 1 (BSE/SE), (**e**,**f**) microstructural detail in zone 2 (BSE/SE).

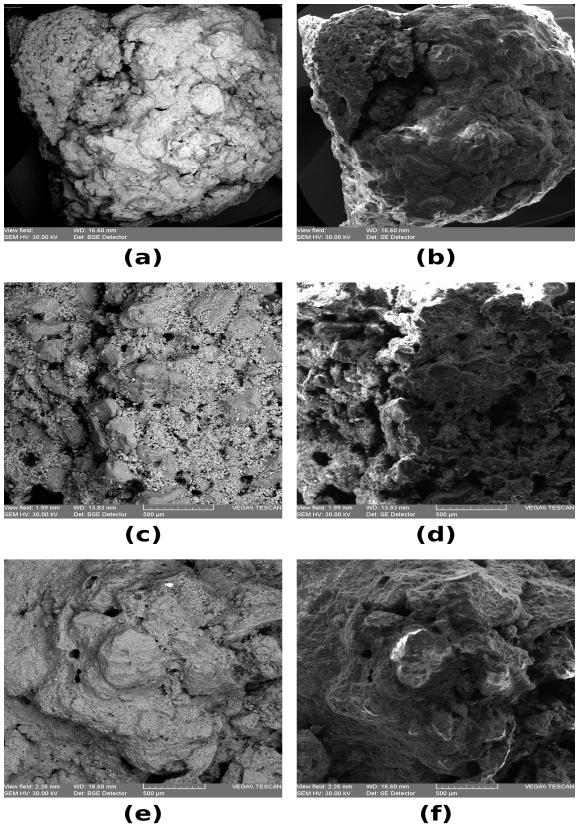


Figure 5. SEM images (BSE and SE) of sample Av at two magnification levels: (**a**,**b**) whole-sample SEM imaging (BSE/SE), (**c**,**d**) microstructural detail in zone 1 (BSE/SE), (**e**,**f**) microstructural detail in zone 2 (BSE/SE).

3.3. FTIR Characterization

FTIR spectroscopy was employed to complement the elemental and microstructural observations obtained by pXRF and SEM–EDX, offering molecular-scale information on carbonate phases, sulfate species and organic residues associated with crust formation. The technique is particularly sensitive to distinguishing unaltered carbonate mortar from sulfated surface layers, consistent with previous studies on heritage materials [27,28]. The raw (as-acquired) FTIR spectra for Nv, Af, and Av are provided in Figure S1, whereas Figure 6 presents the processed spectra with the main band positions highlighted/assigned.

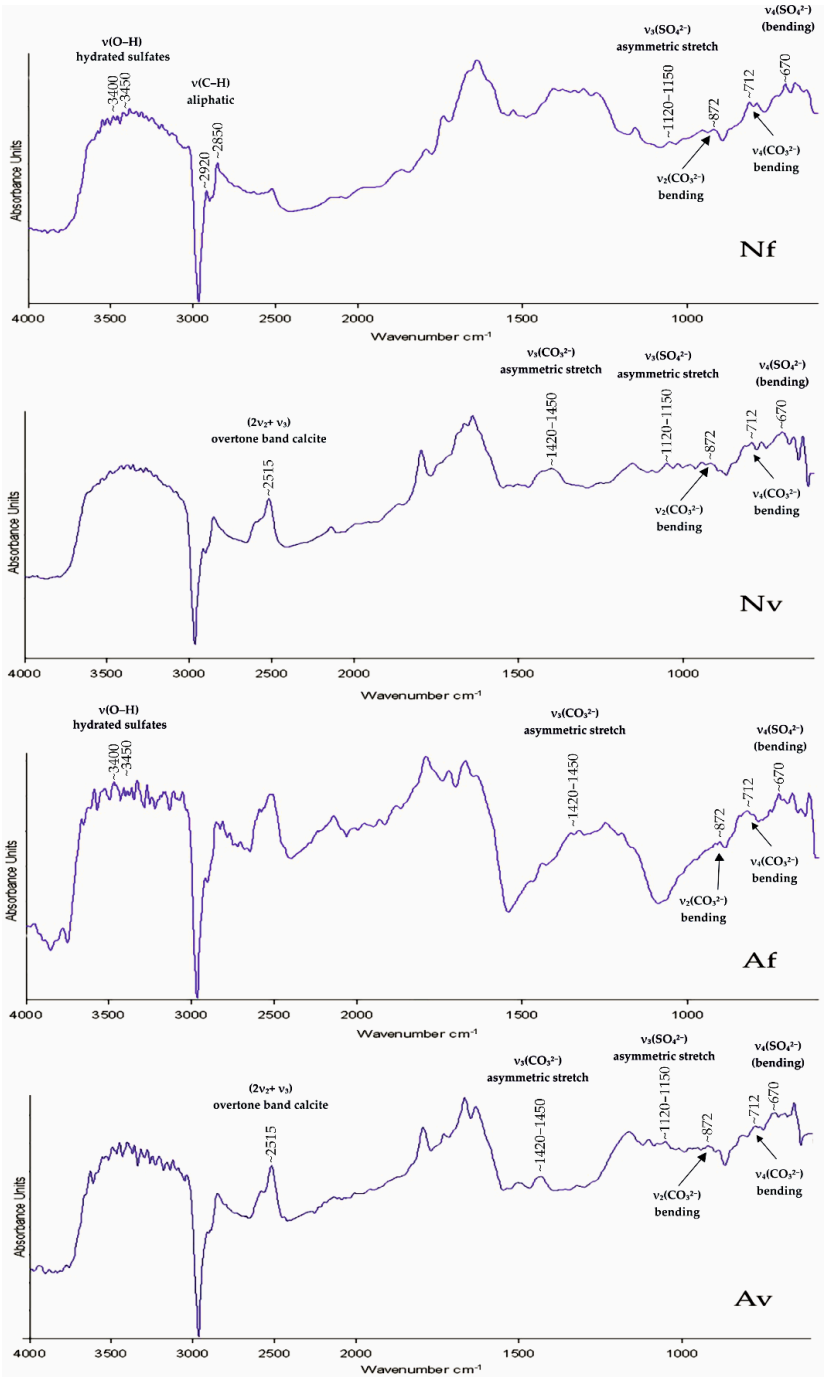
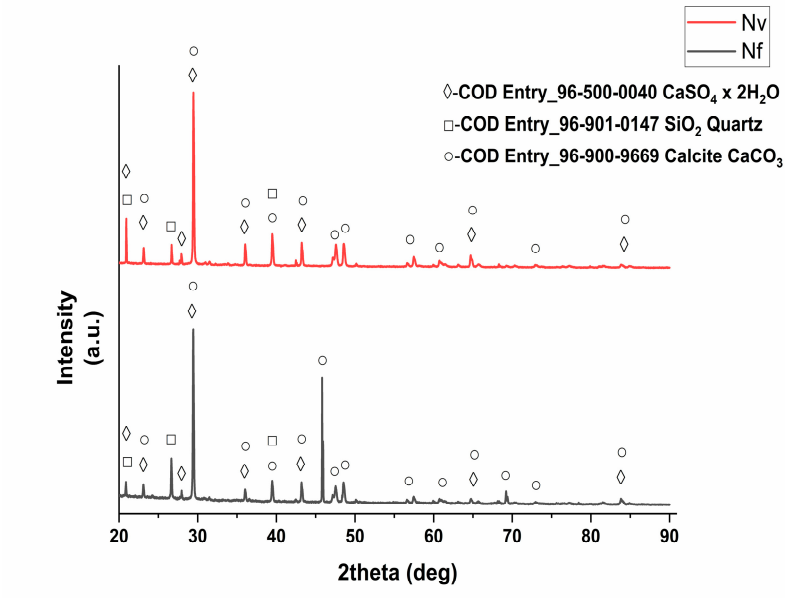


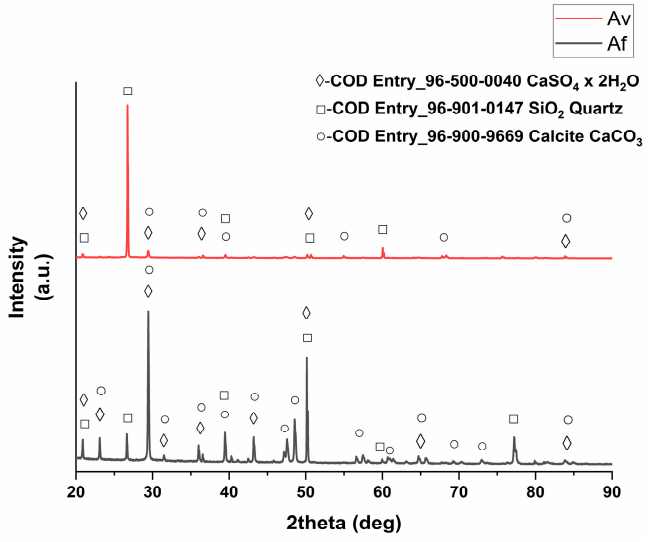
Figure 6. FTIR spectra acquired on the investigated surfaces (Nf; Nv; Af; Av). with bands (4000–600 cm^{-1}) and representative references.

3.4. XRD Characterization

X-ray diffraction was used to investigate the phase composition of each sample. The analysis revealed that all the measured samples consist of a mixture of three phases (Figure 7): quartz SiO_2 (COD entry no. 96-901-0147) [29], calcite CaCO3 (COD entry no. 96-900-9669) [30] and calcium sulfate dihydrate $CaSO_4 \cdot 2H_2O$ (COD entry no. 96-500-0040) [31]. No additional crystallographic phase was detected in the analyzed powders.



(**a**)



(**b**)

Figure 7. XRD patterns of the four mortar surfaces powder samples from the west enclosure wall of Golia Monastery: (**a**) Nf and Nv; (**b**) Av and Af. Peak positions of gypsum ($CaSO_4 \cdot 2H_2O$), quartz (SiO_2), calcite ($CaCO_3$) and are indicated.

3.5. CIE Lab Colorimetric Characterization of the Mortar Surfaces

Colorimetric measurements were performed on the six investigated mortar surfaces—Nf, Nv, Af, Av, and additional Nc and Ac—using the CIE Lab system in order to quantify surface lightness (L^*) and chromatic coordinates (a^*, b^*) at high precision. The number of colorimetric spot measurements varied depending on the investigated surface, as summarized in Table S2. Specifically, five spots were measured on Nf, four on Nv, three on Af, three on Av, three on Nc, and four on Ac. Mean values and standard deviations

were calculated for each surface based on these spot measurements. The raw measurement set includes individual L^*, a^*, b^* triplets for each point, while the processed dataset reports averaged chromatic parameters for all six surfaces. A full ΔE_{00} matrix (6 × 6) was also computed to document the chromatic distances between all possible surface pairs. CIE Lab coordinates and ΔE_{00} color differences were calculated according to the CIE DE2000 definition of the CIE Lab space and Euclidean color distance [32]. The interpretation of ΔE_{00} values in terms of perceptibility thresholds follows published color-difference studies [21,22]. The results presented below summarize the mean CIE Lab values and the corresponding color differences, providing a quantitative basis for the comparative analysis among exposed, protected, and internal mortar domains (Tables 3 and 4).

Table 3. CIE $L^*a^*b^*$ colorimetric parameters (mean ± SD) for the investigated mortar surfaces and corresponding visual interpretation.

Investigated Surfaces [1]	Colorimetric Parameters			Visual Interpretation
	L^*	a^*	b^*	
Nf	30.72 ± 0.45	2.00 ± 0.21	7.59 ± 0.42	heavy darkening; mature black gypsum–soot crust.
Nv	49.89 ± 3.34	3.74 ± 0.15	14.67 ± 0.02	protected verso; minimal alteration.
Af	42.90 ± 0.04	4.48 ± 0.02	14.11 ± 0.07	partial soiling; early-stage alteration.
Av	45.21 ± 1.06	3.55 ± 0.09	12.51 ± 0.07	slightly darker than Nv; still unaltered.
Nc	54.27 ± 1.07	4.10 ± 0.35	15.07 ± 0.95	unaltered lime mortar; optical reference.
Ac	52.98 ± 4.11	4.44 ± 0.35	14.79 ± 0.62	unaltered lime mortar; confirms shared mortar recipe.

[1] Legend: Nf = exposed black-crusted face of sample N; Nv = verso; Af = exposed face of sample A; Av = verso; Nc = inner core of sample N; Ac = inner core of sample A.

Table 4. Matrix (6 × 6) for ΔE_{00} color differences between the six mortar surfaces.

Investigated Surfaces	ΔE_{00} Color Differences					
	Nf	Nv	Af	Av	Nc	Ac
Nf	0	17.63	11.37	12.92	22.10	20.77
Nv	17.63	0	6.84	4.80	4.35	3.18
Af	11.37	6.84	0	2.53	11.33	9.96
Av	12.92	4.80	2.53	0	9.20	7.91
Nc	22.10	4.35	11.33	9.20	0	1.34
Ac	20.77	3.18	9.96	7.91	1.34	0

Lightness (L^*) ranges from 30.72 for Nf to 54.27 for Nc, while a^* values vary between 2.00 and 4.48 and b^* between 7.59 and 15.07. All chromatic coordinates fall in the positive $a^* - b^*$ quadrant, corresponding to reddish–yellowish hues typical of lime mortars. The ΔE_{00} matrix in Table 4 shows the largest color differences between Nf and the inner-core surfaces (Nc, Ac) and the smallest differences between Nc and Ac and between Nv and Ac. For orientation, a standard observer sees the difference in color as follows [33]:

- $0 < \Delta E < 1$—the observer does not notice the difference;
- $1 < \Delta E < 2$—only an experienced observer can notice the difference;
- $2 < \Delta E < 3.5$—an unexperienced observer also notices the difference;
- $3.5 < \Delta E < 5$—a clear difference in color is noticed;

- 5 < Δ*E*—the observer notices two different colors.

3.6. Optical Microscopy (OM) of Mortar Microtextures

Optical microscopy (OM) provides direct visual evidence of microtextural variations between exposed, partially exposed, and unexposed mortar surfaces, complementing the chemical and structural information obtained through pXRF, SEM–EDX, FTIR, and colorimetry. At the scale of several hundred micrometers, OM is particularly useful for assessing (i) the presence and distribution of dark particulates (soot-like carbonaceous deposits), (ii) early and advanced crystallization of alteration minerals (e.g., gypsum microcrystals), (iii) binder–aggregate interactions and mortar integrity, (iv) biological microfilms and surface contamination, and (v) differences between exterior faces, verso faces, and inner core materials, in line with previous applications of optical microscopy to historic lime mortars and masonry decay [34–36]. In the context of the two analyzed mortar fragments (samples N and A), OM makes it possible to identify a clear morphological alteration gradient between exposed faces (Nf, Af), protected faces (Nv, Av), and inner core materials (Nc, Ac). The OM observations for Nf, Nv, Af, Av, Nc, and Ac are presented below to enable a side-by-side comparison of microtextures and alteration markers (soot, gypsum, porosity, biofilm) across exposed, protected, and core materials (Figure 8).

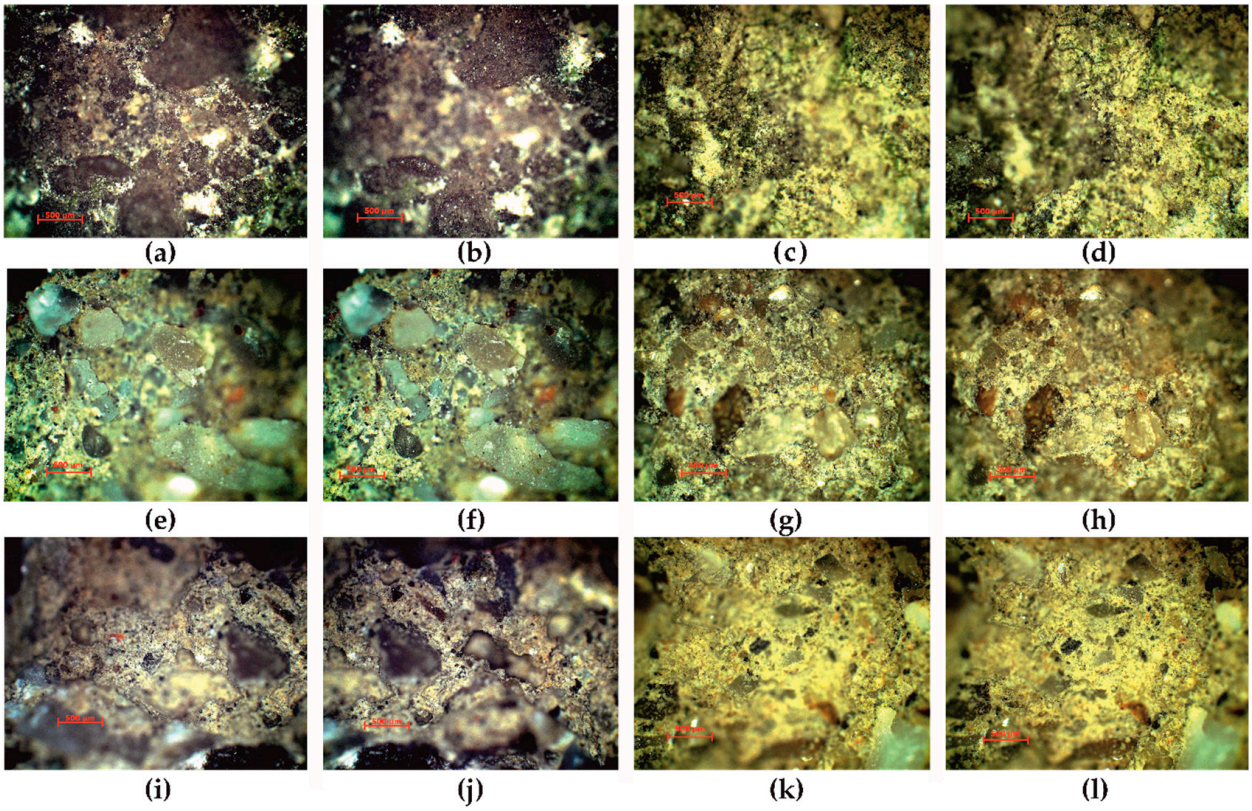


Figure 8. Optical microscopy (OM) panel of the four main mortar surfaces (Nf, Nv, Af, Av) and the two inner-core reference surfaces (Nc, Ac). Each surface is shown through two micrographs captured at slightly different focal distances: (**a**,**b**) Nf; (**c**,**d**) Nv; (**e**,**f**) Af; (**g**,**h**) Av; (**i**,**j**) Nc; (**k**,**l**) Ac.

4. Discussion

The integrated analytical approach applied to mortar samples from the western enclosure wall of the Golia Monastery provides a detailed picture of how urban pollution influences the formation of crust on the surface of the material. The results obtained by pXRF, SEM-EDX, FTIR, XRD, OM and CIE Lab colorimetry converge towards a consistent

interpretation of the alteration gradient observed between the exposed faces (Nf, Af), the protected reverse surfaces (Nv, Av) and the inner core references (Nc, Ac). In this section, the results are interpreted in relation to established mechanisms of sulfation, particulate deposition, and mortar decay.

4.1. pXRF Characterization of Black Crusts and Mortar Alteration

4.1.1. Major-Element Contrasts: Particulate Loading vs. Chemical Sulfation

The mean pXRF compositions (Table 1) highlight two partially decoupled surface processes: (i) silicate particulate accumulation and (ii) surface-directed sulfation of the carbonate binder.

(i) Silicate particulate accumulation (dust loading). A first signal is the accumulation of silicate-rich particles on exposed faces, best tracked by the SiO_2/Al_2O_3 ratio, which is notably higher on the exposed surfaces (Nf = 11.01, Af = 12.25) than on the protected/inner-facing surfaces (Nv = 4.18, Av = 5.36). Elevated SiO_2/Al_2O_3 values suggest that the silicate fraction on exposed areas is comparatively quartz-rich (relative to aluminosilicates), consistent with the deposition of mineral dust in a roadside urban setting. This particulate input also contributes to higher absolute SiO_2 contents on exposed faces, especially on Nf (SiO_2 = 48.81 wt.%).

(ii) Surface-directed sulfation (chemical alteration of the binder). A second, distinct signal is the chemical transformation of the carbonate binder, tracked by the strong contrast in S/Ca. The black-crusted surface Nf exhibits the highest sulfur content (S = 0.58 wt.%) and the highest S/Ca ratio (=0.050), whereas Nv and Af show much lower values (both 0.010) and Av remains intermediate (0.030). Importantly, Nf is also the most Ca-depleted surface (Ca = 12.39 wt.%), while the other surfaces show substantially higher Ca contents (Nv − Ca = 25.55 wt.%, Af − Ca = 23.89 wt.%, Av − Ca = 21.03 wt.%). This combination—Ca depletion + S enrichment + elevated S/Ca—is consistent with preferential surface sulfation and partial conversion of the original carbonate binder into a gypsum-rich alteration layer ($CaSO_4 \cdot 2H_2O$), as widely reported for black crusts on carbonate substrates exposed to SO_2-rich urban atmospheres [2,26].

Integrating the ratios: why Nf is different from Af.

The joint use of SiO_2/Al_2O_3 and S/Ca clarifies that particulate deposition and sulfation do not scale identically across surfaces. Af shows a high SiO_2/Al_2O_3 ratio (12.25), indicating substantial quartz-rich dust loading, yet its S/Ca remains low (0.010), suggesting only incipient sulfation and the absence of a mature gypsum-rich rind. By contrast, Nf concentrates both signals: high SiO_2/Al_2O_3 (11.01) and the highest S/Ca (0.050), indicating that the black crust reflects co-accumulation of particulate matter and advanced chemical alteration. The SiO_2/Ca ratio further summarizes this divergence: Nf reaches 3.94, while the other surfaces remain near unity (Nv 1.05, Af 1.06, Av 1.24), consistent with a surface layer where silicate-rich deposits are superimposed on—and coupled to—carbonate-binder depletion.

In this context, the buttress location along the heavily trafficked George Enescu Street provides a plausible source of both particulate matter (driving the high SiO_2/Al_2O_3 on exposed faces) and Sox (driving high S/Ca on Nf). The marked contrast between the strongly sulfated Nf and the weakly altered Nv/Af/Av is therefore interpreted as a traffic-related pollution imprint, modulated by local exposure and airflow towards the west enclosure wall of Golia Monastery, consistent with the use of gypsum-rich black crusts as passive samplers of ambient air quality in other urban heritage sites [2,26].

4.1.2. Trace Metals as Non-Diagnostic Indicators in This Case Study

Trace metals typically associated with urban emissions (Zn, Pb, Cu, Cr, Sn, V, Zr) are consistently close to or below the detection limit of the applied pXRF configuration ($\leq$0.03 wt.%) on all four surfaces. Within this analytical uncertainty, no systematic enrichment of Zn, Pb or other metals is observed on the black-crust surface Nf relative to the verso surfaces Nv and Av or to the less altered exposed face Af. Lead, for example, is detected at 0.01 wt.% in some verso measurements, while remaining below detection on Nf and Af.

These very low concentrations and the absence of a coherent spatial pattern suggest that the recorded trace metals largely reflect a mixture of lithogenic background and minor, diffuse anthropogenic inputs, rather than a focused accumulation within the black crust. This behavior contrasts with a number of urban case studies in which black crusts incorporate appreciable amounts of heavy metals and carbonaceous particles and can be used as archives of local industrial or traffic pollution [1,2]. By contrast, Fe and Ti display relatively stable concentrations across the four surfaces (Fe = 0.68–1.95 wt.%, Ti = 0.02–0.15 wt.%), supporting their predominantly lithogenic origin. The main alteration marker in this case is therefore the sulfur enrichment and S/Ca ratio on Nf, rather than any distinctive trace-metal signature.

4.1.3. Behavior of Chlorine (Cl) in the pXRF Datasets

Chlorine is detected at very low levels (generally 0.08–0.20 wt.%) and only at some of the measured spots. A small but reproducible signal occurs on Af (mean Cl = 0.20 wt.%), whereas Nv and Av show sporadic occurrences (0.08–0.10 wt.%), and Cl remains below detection on the black-crusted Nf surface (Table 1).

Given these concentrations and the known limitations of handheld and portable XRF instruments for quantifying halogens—especially Cl—under standard oxide calibrations, the reported values must be regarded as qualitative rather than strictly quantitative [37,38]. The low but reproducible Cl on Af is consistent with minor chloride deposition or retention at the exposed surface (e.g., urban aerosols, road-splash water or de-icing residues [6]), while the scattered signals on Nv and Av may reflect partial internal redistribution within the porous mortar.

Crucially, however, there is no evidence of Cl enrichment on Nf compared with the other surfaces, and all values lie near the detection threshold. Chlorine can therefore be considered a secondary, non-diagnostic component in this case: it does not appear to exert a primary control on black crust formation, which is overwhelmingly governed by sulfur-driven gypsum precipitation.

4.1.4. Behavior of Phosphorus (P) and Implications for Bioreceptivity

Phosphorus occurs at very low concentrations on all four surfaces, with mean values between 0.05 and 0.11 wt.% (Table 1), i.e., close to the detection limit of the pXRF configuration used. This range is typical for lime-based mortars, where P is not an intentional component and usually reflects minor impurities, occasional deposition of organic matter or guano, or incipient biological colonization. No systematic difference is observed between exposed (Nf, Af) and verso (Nv, Av) surfaces: P remains low and broadly similar on all of them, indicating that phosphate-bearing phases do not control the chemical contrast between black-crusted and non-crusted areas, in contrast to sulfur.

Nevertheless, the consistent, albeit weak, presence of P on all surfaces is compatible with the development of early lithobiontic communities (e.g., microbial biofilms, fungi, algae or lichens) on and within the mortar, especially when considered together with microscopic evidence of biogenic films described elsewhere in this study. Phosphorus-

bearing biominerals and organo-mineral coatings are increasingly recognized as part of the wider family of alteration layers on stone monuments and as sensitive recorders of local environmental change [38]. In this sense, the low but measurable P contents on the Golia mortars may be viewed as a subtle signal of bioreceptivity under the present urban microclimate—an additional "temporal fingerprint" of pollution-related change, superimposed on the dominant sulfur-related gypsum crust. Although P intensities remain close to the handheld XRF detection limit, the weak but systematic enrichment of phosphorus on the black-crusted faces can be tentatively linked to lithobiontic colonization and the trapping of P-rich atmospheric particulates. Phosphorus is a key nutrient for microbial biofilms on stone surfaces, which are known to benefit from ammonium and phosphate supplied by atmospheric deposition, and Ca–phosphate particles have been repeatedly reported within gypsum-rich urban black crusts as markers of anthropogenic pollution [1,39].

4.2. Discussion of SEM–EDX Results

Scanning electron microscopy coupled with energy-dispersive X-ray spectroscopy (SEM–EDX) was employed to investigate the microstructural and elemental signatures associated with crust development, surface alteration and mortar preservation. SEM–EDX provides high-resolution imaging of surface textures (secondary electrons, SE; backscattered electrons, BSE) and quantitative elemental data at the micrometer scale, thereby complementing pXRF and FTIR observations on sulfation, gypsum formation, particle deposition and binder degradation. Black layers and black crusts are widely recognized as a typical alteration form on carbonate heritage exposed to polluted urban atmospheres and commonly consist of gypsum with embedded carbonaceous and mineral particles [1,40,41].

Across the four analyzed faces (Nf, Nv, Af, Av), and for both SEM–EDX micro-areas on each face (zone 1 and zone 2), the data reveal a consistent distinction between exposed and protected surfaces, reflecting an alteration gradient driven by atmospheric pollution and moisture-mediated reactions at the wall–air interface (Tables 2 and 5).

Table 5. SEM–EDX-based microstructural and chemical characterization of the four investigated mortar surfaces. (Nf, Nv, Af, Av), summarizing key elements, diagnostic features, and inferred alteration stages.

Surface	Microstructure (SEM–SE/BSE)	Key Elements (EDX)	Alteration Stage	Diagnostic Features
Nf (black-crusted face)	heterogeneous, porous surface; outer texture partly masked by dark particulates and bright Ca–S microcrystals	high O and Si; lower Ca than verso; minor S, Al, Fe, K, Mg; carbonaceous aggregates	advanced alteration	particulate-rich blackened skin with scattered gypsum microcrystals; partial masking of binder–aggregate contacts
Nv (verso of N)	clean, compact calcitic matrix; open porosity; limited adherent particles; no continuous secondary phases	high Ca, moderate Si and Al; S only at minor levels	unaltered	lime-mortar texture preserved; no continuous crust
Af (exposed but non-blackened)	matrix clearly visible; scattered particles and isolated microcrystals at pore edges; early pore-mouth deposits	high Ca, moderate Si; very low S and Cl; minor Al and Fe	early alteration	incipient sulfate and dust deposition; binder–aggregate structure largely preserved
Av (verso of A)	uniform calcitic texture; sharp grain boundaries; local Si-rich patches but no continuous deposits.	Ca-rich mortar with moderate Si; S present only at minor levels	slightly altered/largely unaltered verso	clean verso reference for sample A, with only limited dust accumulation

4.2.1. Nf—SEM–EDX of the Blackened Exposed Surface

The Nf surface displays a heterogeneous micro texture dominated by fine particulate accumulations that coat the outer mortar. In SE images, both Nf zones show irregular dark grains filling or bridging pore openings, whereas BSE imaging reveals a patchy network of brighter high-Z spots associated with Ca- and S-bearing microcrystals. These clusters are concentrated along pore walls and micro-cavities, indicating preferential nucleation sites at the air-exposed interface.

EDX analyses for Nf zones 1 and 2 are characterized by high O and Si and clearly reduced Ca contents compared with the verso surfaces, while S occurs only as a minor but persistent constituent together with Al-, Mg- and Fe-bearing inclusions. The two micro-areas reproduce this trend, with zone 2 slightly more Si- and S-rich, consistent with a dust-rich pocket within the outer skin. Overall, the Nf face corresponds to a siliceous, particulate-rich blackened layer embedding thin Ca–S micro precipitates rather than a continuous massive gypsum crust. Such arrangements of Ca–S crystals intergrown with soot and mineral dust are typical of urban black crusts described elsewhere [40,42].

4.2.2. Nv—SEM–EDX of the Verso (Protected) Surface

The Nv surface, corresponding to the verso of sample N, retains a more preserved mortar fabric. SEM images of both Nv zones show a compact, light-toned calcitic matrix with well-defined binder–aggregate contacts, open and largely unclogged porosity, and clean grain boundaries with only scarce adherent particulates. No continuous secondary phase is observed along the outermost pores.

EDX spectra for Nv zones 1 and 2 are dominated by Ca and O, with moderate Si and Al associated with quartz and aluminosilicate phases, and only very low S contents close to the detection threshold. This micro texture corresponds to a largely unaltered lime mortar, in agreement with FTIR signatures dominated by calcite and with the higher L^* values obtained by colorimetry. Nv therefore behaves as an internal reference substrate for sample N, representing the mortar prior to significant atmospheric alteration.

4.2.3. Af—SEM–EDX of the Exposed but Non-Blackened Surface

The Af surface exhibits intermediate features between the heavily polluted Nf face and the preserved Nv verso. In SE and BSE images, the two Af zones show fine, scattered dark particulates within pores and along microcracks, but these do not form a continuous film. Sparse bright spots are visible in BSE mode and correspond to small Ca- and S-bearing precipitates, which are much less abundant than on Nf. The mortar matrix remains clearly recognizable, with binder–aggregate contacts largely intact and significant portions of the pore network still open.

EDX data for Af zones 1 and 2 confirm Ca as a major constituent, together with moderate Si and Al and only low S and Cl contents. This pattern indicates a carbonate mortar that has incorporated limited atmospheric dust and incipient sulfate phases, but without extensive decalcification or crust consolidation. Af thus represents an early stage of sulfation and particulate accumulation, consistent with weaker FTIR sulfate bands and moderate color shifts compared to the blackened Nf surface.

4.2.4. Av—SEM–EDX of the Verso Surface

The Av verso surface of sample A closely resembles Nv in both morphology and composition, although with slightly higher micro-scale variability between the two investigated areas. SEM images show a clean calcitic matrix, sharp aggregate boundaries and open porosity, with only isolated deposits along pore edges and no evidence of a continuous secondary layer.

EDX spectra for Av zones 1 and 2 confirm the dominance of Ca with moderate Si and Al. Sulfur remains at minor levels, although one of the micro-areas shows slightly higher Si and lower Ca, pointing to a thin Si-rich deposit superimposed on a Ca-rich mortar substrate. As for Nv, the absence of well-developed sulfate crystals or pervasive particulate infilling indicates a limited environmental impact on this protected face. Av therefore acts as the internal reference for sample A, analogous to Nv for sample N.

4.2.5. Comparative Microstructural Synthesis (Nf, Nv, Af, Av)

Cross-comparison of SEM–EDX data for zones 1 and 2 on all four faces reveals a clear surface-directed alteration gradient (Tables 2 and 5):

- Strongly altered (Nf)—both zones show particulate accumulations and low bulk Ca, with thin Ca–S micro precipitates and locally obscured binder–aggregate contacts forming a heterogeneous blackened skin.
- Moderately altered (Af)—scattered particulates and isolated sulfate microcrystals occur in both zones, but the mortar matrix remains visible and no continuous crust is observed.
- Slightly altered/protected (Nv, Av)—zones 1 and 2 on the verso faces retain clean, Ca-rich mortar textures with open porosity, limited dust deposits and only minor S signals.

This microstructural gradient mirrors the pXRF S/Ca patterns and the relative intensity of sulfate bands in FTIR spectra, providing a direct link between bulk-scale chemical contrasts and microscale textural changes at the mortar surface.

4.2.6. Discussion of SEM–EDX Results

Overall, SEM–EDX indicates that alteration processes are predominantly surface-confined, affecting only the outermost tens of micrometers of the mortar, with no evidence for deep decalcification fronts in any of the investigated zones. The occurrence of Ca–S microcrystals and minor S enrichment on the exposed faces (Nf, and, to a lesser extent, Af) supports a sulfate-forming mechanism controlled by atmospheric SO_x and humidity cycles, with precipitation preferentially located at pore mouths and along microcracks, in line with mechanisms described for gypsum-rich black crusts on carbonate heritage [1,40].

The associated carbon-rich particulates observed on Nf are consistent with traffic-derived soot and other combustion aerosols, as commonly reported in black crusts acting as passive samplers of urban air pollution [1,2,42]. This interpretation agrees with the position of the west enclosure wall of Golia Monastery along George Enescu Street, a corridor of intense vehicular circulation.

By contrast, the verso surfaces (Nv, Av) and inner cores retain the textural and chemical features of a lime-based mortar with only marginal sulfate signals, underscoring the strong directionality of alteration and the primary role of exposure geometry and local microclimate in controlling crust development on the Golia wall. Similar exposure-controlled gradients between blackened and sheltered areas have been highlighted in other urban heritage sites, reinforcing the view that sulphation and soiling processes are tightly coupled to pollutant pathways and moisture regimes at the stone–atmosphere interface [41,43].

4.3. FTIR Results and Spectral Interpretation

The FTIR analysis provides a detailed molecular-scale view of the alteration processes affecting the four investigated surfaces (Nf, Nv, Af, Av). The spectra cover the diagnostic 4000–600 cm^{-1} region and enable clear distinction between carbonate-dominated unaltered mortars, gypsum-bearing black crusts and surfaces at intermediate stages of alteration. The principal vibrational features identified (Figure 6, Table 6) correspond to calcite, gypsum,

hydrated phases and organic or soot-like residues, in agreement with FTIR characterizations reported for historical mortars and atmospheric crusts.

Table 6. Summary of diagnostic FTIR bands (4000–600 cm^{-1}) with representative references.

Wavenumber (cm^{-1})	Assignment	Interpretation	Presence in Surfaces	Representative References
~3400–3450	ν(O–H)	hydrated sulfates/gypsum	strong in Nf weak in Af absent in Nv/Av	[44]
~2920, ~2850	ν(C–H) aliphatic	soot-like organics urban aerosols	visible in Nf	[45]
~2515	combination overtone band ($2\nu_2 + \nu_3$) of calcite	indicator of well-crystallized $CaCO_3$	strong in Nv/Av weakened in Nf	[46]
~1420–1450	$\nu_3(CO_3^{2-})$ asymmetric stretch	carbonate backbone (calcite)	dominant in Nv/Av/Af subdued in Nf	[47–49]
~1120–1150	$\nu_3(SO_4^{2-})$ asymmetric stretch	hydrated gypsum/ sulfate-rich alteration	strong in Nf weak in Af minimal in Nv/Av	[44]
~872	$\nu_2(CO_3^{2-})$ bending	carbonate matrix	strong in Nv/Av/Af reduced in Nf	[49]
~712	$\nu_4(CO_3^{2-})$ bending	calcite signature	strong in Nv/Av/Af reduced in Nf	[49]
~670	$\nu_4(SO_4^{2-})$ (bending)	gypsum	strong in Nf weak in Af minimal in Nv/Av	[44]

A comparative reading of the spectra highlights the contrast between protected verso zones (Nv, Av) and exposed faces (Nf, Af), enabling a stratigraphic interpretation of deterioration patterns, similar to approaches reported in urban heritage environments [1,40,50,51].

4.3.1. FTIR Analysis of Nf (Black-Crusted Surface)

The Nf spectrum shows the characteristic fingerprint of a gypsum-rich black crust. A broad O–H stretching envelope (~3400–3450 cm^{-1}) [44] confirms the presence of hydrated salts/sulfates, as typically observed in salt-rich crusts formed under polluted urban atmospheres. The strong absorptions at ~1120–1150 cm^{-1} $\nu_3(SO_4^{2-})$ and ~670 cm^{-1} $\nu_4(SO_4^{2-})$ indicate abundant gypsum [44], in line with studies demonstrating the dominance of calcium sulfate in mature black crusts. Weak but detectable C–H stretching bands (~2920, ~2850 cm^{-1}) [45] point to the incorporation of soot and organic particulates, a recurrent feature in traffic-exposed crusts. The attenuation of calcite bands further confirms surface masking by sulfate accretions.

4.3.2. FTIR Analysis of Nv (Inner Reference Mortar)

The Nv verso spectrum is representative of an unweathered lime-based mortar dominated by calcite. The CO_3^{2-} combination band at ~2515 cm^{-1} and the well-defined calcite modes ν_3 (~1420–1450 cm^{-1}), ν_2 (~872 cm^{-1}) and ν_4 (~712 cm^{-1}) are consistent with the spectral signatures of historical carbonate mortars. Only minimal sulfate signals are detected, indicating negligible sulfation penetration—an expected behavior for protected substrate zones.

4.3.3. Comparative Interpretation: Nf vs. Nv

The superimposed spectra of Nf and Nv highlight the transition from an intact calcitic substrate (Nv) to a gypsum-rich, pollution-derived crust (Nf). Nf shows intensified sulfate peaks (~1120–1150 and ~670 cm^{-1}) and a reduction in carbonate intensities, mirroring the crust–substrate relationships reported in urban-exposed monuments.

In contrast, Nv preserves the full calcite triplet with only trace sulfate presence. The spectral divergence confirms a shallow, surface-confined sulfation process typical of polluted façades.

4.3.4. FTIR Analysis of Av (Verso Substrate)

The Av verso spectrum closely resembles Nv, with pronounced carbonate bands—ν_3 (~1420–1450 cm^{-1}), ν_2 (~872 cm^{-1}) and ν_4 (~712 cm^{-1})—and only weak or incipient sulfate features. This reflects a well-preserved, largely unaltered mortar analogous to protected zones reported in the literature [49]. The absence of significant O–H or C–H features confirms minimal exposure to moisture fluctuations or organic pollutants.

4.3.5. FTIR Analysis of Af (Exposed but Non-Blackened Face)

The Af spectrum is primarily carbonate-dominated but displays subtle enhancement of sulfate modes relative to Av. Slight broadening in the O–H region suggests moisture retention and early-stage gypsum formation, indicative of an initial alteration front rather than a fully developed crust. This pattern aligns with early atmospheric alteration in exposed but non-blackened mortar surfaces.

4.3.6. Comparative Interpretation: Af vs. Av

Comparing Af and Av reveals limited but measurable atmospheric impact on Af. Elevated sulfate signals, slight attenuation of carbonate peaks, and broader O–H absorptions indicate incipient sulfation consistent with early alteration stages described in urban environments. Av remains a clean carbonate reference, confirming that the observed changes in Af derive from direct environmental exposure rather than intrinsic mortar variability.

4.3.7. Comparative Interpretation: Nf vs. Af (Crust vs. Exposed Non-Blackened Surface)

The contrast between Nf and Af provides insight into the progression from early sulfation (Af) to fully developed gypsum crusts (Nf). While both surfaces exhibit sulfate features, Af displays only moderate $\nu_3(SO_4^{2-})$ (~1120–1150 cm^{-1}) intensities and retains strong carbonate peaks, indicating partial surface alteration.

In contrast, Nf shows dominant sulfate absorptions, subdued carbonate modes, broad O–H stretching, and detectable C–H bands—signatures characteristic of black crusts enriched in gypsum and organic particulates.

This spectral gradient mirrors the typical evolution of exposed calcareous mortars under sustained atmospheric pollution: initial sulfate nucleation (Af), followed by progressive gypsum accumulation, hydration, and incorporation of airborne particulates (Nf) as documented in heritage façades across polluted cities.

4.4. CIE Lab—Colorimetric Signatures of Black Crust Formation and Mortar Alteration

The CIE Lab dataset reveals systematic color contrasts between the black-crusted faces, the protected verso areas and the inner-core mortars (Tables 3 and 4). The exposed Nf surface shows the lowest lightness (L^* = 30.72) and the lowest b^* value (7.59), indicating a markedly darker and less yellow appearance than all other surfaces. In contrast, the inner cores Nc and Ac exhibit the highest lightness (L^* = 54.27 and 52.98, respectively) and relatively high b^* values (15.07 and 14.79), consistent with cream-colored lime mortars.

Verso surfaces (Nv, Av) and the exposed face Af occupy an intermediate position in L^*, suggesting partial darkening but without the strong loss of chroma observed for Nf.

The ΔE_{00} (6 × 6) matrix further quantifies these contrasts. Color differences involving Nf are systematically high, with ΔE_{00} values of 17.63 (Nf–Nv), 11.37 (Nf–Af), 12.92 (Nf–Av), 22.10 (Nf–Nc) and 20.77 (Nf–Ac) (Table 4). According to commonly used perceptibility ranges in CIE Lab space, when ΔE_{00} values are located between 1 and 2, only experienced observers can notice the difference. Also, when ΔE_{00} varies from 3 to 5 units, a clear difference in color is noticed, and when $\Delta E_{00} > 5$ units, the observer notices two different colors [33]. The Nf surface therefore represents a chromatically distinct state relative to both its verso and core counterparts. In contrast, the color difference between the two inner cores (Nc–Ac, $\Delta E_{00} = 1.34$) falls below the threshold of clear visual detection, and pairs such as Nv–Ac ($\Delta E_{00} = 3.18$) or Af–Av ($\Delta E_{00} = 2.53$) lie in the range of small but perceptible shifts (Table 4).

These patterns are consistent with colorimetric signatures reported for black crusts and pollution-related soiling on carbonate stone. Studies on architectural limestones exposed to SO_2 attack and particulate deposition have documented decreases in b^* and L^* results and modifications of chroma and lightness, particularly in the yellow component, as crusts develop and dark particles accumulate [52]. Similarly, color-based analyses of black layers on heritage limestones in Madrid have linked darker L^* values and altered façade color patterns to successive episodes of air pollution and cleaning [53].

In a broader conservation context, colorimetric monitoring of architectural heritage has shown that ΔE_{00} values above about 5 units are generally taken as an upper limit for acceptable chromatic alteration induced by treatments or soiling, beyond which changes become visually obvious to observers. Within this framework, the ΔE_{00} values measured between Nf and the inner-core mortars (≈20.77–22.10) place the black-crusted surface far beyond typical acceptability thresholds used in stone conservation, whereas verso and core zones remain chromatically close. The colorimetric indicates that the underlying mortars retain color characteristics typical of fresh lime-based materials, with the alteration restricted primarily to the exposed face. At the same time, the very low ΔE_{00} between Nc and Ac indicates that both cores can serve as an internal chromatic reference when evaluating future cleaning or replacement interventions on the Golia enclosure wall.

These colorimetric gradients mirror the chemical and microstructural contrasts discussed in Sections 4.1–4.4, reinforcing the interpretation of Nf as the most advanced stage of pollution-driven alteration.

4.5. Optical Microscopy and CIE Lab Color Gradients in the Mortar Surfaces

Optical microscopy (OM) confirms that the chromatic contrasts quantified by the CIE Lab dataset reflect distinct microtextural states of the investigated mortar surfaces. In line with applications of OM to historic lime mortars, the micrographs resolve variations in matrix brightness, particulate loading and pore visibility that can be directly related to measured lightness (L^*) and color differences ΔE_{00} between exposed, verso and inner-core zones (Figure 8; Tables 3 and 4).

The exposed black-crusted face Nf displays a continuous darkened veneer with abundant opaque particulates that partly obscure the underlying lime matrix and fill surface-connected pores (Figure 8a,b). This microtextural darkening is consistent with the very low L^* (30.72) and reduced b^* (7.59) values, as well as with the very large ΔE_{00} distances between Nf and all other surfaces (≈11.37–22.10 units), indicating a shift toward a distinctly different color state. Similar combinations of strong lightness loss, decreased yellow chroma and dense accumulations of pollution-derived particles have been reported for blackened architectural limestones subjected to SO_2 attack and urban soiling [53].

Verso surfaces (Nv, Av) (Figure 8c,d,g,h) and the exposed face Af (Figure 8e,f) show more heterogeneous microtextures, with patchy darkened zones, localized accumulations of fine particulates and areas where the bright binder and coarse aggregates remain clearly visible. The partial masking of the matrix corresponds to intermediate L^* values (≈42.90–49.89) (Table 3) and to moderate ΔE_{00} values when these surfaces are compared with the inner cores (≈1.34–11.33 units) (Table 4), which fall in the range of small yet perceptible chromatic shifts. These features are typical of surfaces affected by incipient black crust development and non-uniform soiling, where colorimetric changes track the progressive coverage of the original mortar by particulate-rich layers [52].

In contrast, the inner-core mortars Nc and Ac (Figure 8i–l) exhibit bright, relatively homogeneous matrices with well-defined aggregate grains and open pores, and only minor dark specks. This morphology is compatible with their high L^* (54.27 and 52.98) and high b^* values (15.07 and 14.79) (Table 3), characteristic of cream-colored lime mortars, and with the very small ΔE_{00} between Nc and Ac (1.34) (Table 4), below the threshold of clear visual detection. Such protected or internal zones are widely used as chromatic references when evaluating surface treatments and pollution-induced soiling on stone and mortar substrates, as they preserve the closest approximation to the original hue and lightness [54,55].

Taken together, the OM observations and the CIE Lab parameters depict a coherent alteration gradient: from a heavily darkened, particulate-rich crust on Nf, through partially soiled and chromatically shifted verso and exposed faces (Nv, Av, Af), to relatively unaltered inner-core mortars (Nc, Ac). The close correspondence between microtextural darkening and decreasing L^*, as well as between progressive masking of the matrix and increasing ΔE_{00}, confirms that colorimetry provides a robust quantitative proxy for the visually assessed state of crust development and soiling on the Golia mortar surfaces.

4.6. Synthesis and Integrated Interpretation: Black Crust Evolution and Conservation Implications

Comparable pollution-driven alteration patterns have been reported for other historic masonry structures in Iași, where particulate deposition, surface darkening, and micro-stratigraphic crust development were documented on various geomaterial substrates [6,13,14,56]. These regional analogs reveal a consistent trend of pollution-induced alteration across Iași's historical architecture, thereby strengthening the interpretive framework for the mortars of the Golia Monastery enclosure wall.

At the same time, the interpretative framework adopted here aligns with contemporary artefactometric assessment principles, which advocate rigorous quantification and the integration of multi-parameter diagnostic grids for evaluating deterioration processes in cultural heritage materials [57].

4.6.1. Multi-Analytical Reconstruction of the Alteration Pathway

The combined pXRF, SEM–EDX, FTIR, XRD, CIE Lab colorimetry and OM results converge towards a coherent picture of pollution-driven alteration affecting the restoration mortars on one of the western enclosure buttresses of Golia Monastery, most likely applied during the 2008–2010 intervention campaigns. At this relatively short exposure timescale (≈15 ÷ 17 years), the analytical evidence shows that the outer millimeters of the joints have already experienced marked chemical, mineralogical, microstructural and chromatic change, while the inner cores still preserve the features of a lime-based repair mortar.

From a chemical standpoint, pXRF points to a surface-directed sulfation pattern centered on the blackened Nf face: higher S contents and elevated S/Ca ratios distinguish Nf from Af, Nv and Av, in agreement with partial conversion of the carbonate binder into sulfate phases at the air–mortar interface. Trace metals (Zn, Pb, Cu) remain close to or below the detection limit and do not define a diagnostic pollution signature [1], whereas

low but measurable P contents across all surfaces suggest early lithobiontic colonization superimposed on the sulfur-driven crust, in line with recent discussions of phosphate-bearing biofilms on stone monuments [58].

SEM–EDX and OM translate these bulk signatures into microstructural states. Nf is characterized by a particulate-rich blackened skin, partial masking of binder–aggregate contacts and locally sealed porosity. Af shows only scattered particulates and isolated sulfate microcrystals, consistent with an early alteration stage (Figures 2 and 8a,b). By contrast, Nv and Av retain bright, Ca-rich matrices with open pores and limited dust accretions, behaving as largely preserved verso substrates for samples N and A (Figures 2 and 8c,d,g,h). These observations match typical micro textures reported for urban black crusts, where gypsum and soot accumulate preferentially at exposed surfaces [59].

FTIR spectra for Nf provide direct confirmation of a gypsum-rich black crust, with strong sulfate bands and O–H absorptions indicative of hydrated sulfates, accompanied by weak C–H stretching bands that reflect soot and organic particulates. Nv and Av are carbonate-dominated and act as spectral references for unaltered lime mortar, while Af exhibits intermediate features consistent with incipient sulfation. This stratigraphic contrast between Nf and Nv/Av reproduces crust–substrate relationships described for calcareous façades in polluted environments [59].

Colorimetric data integrate these changes into a perceptual scale. Nf exhibits the lowest lightness (L^* = 30.72) and reduced b^* (7.59), whereas Nc and Ac display high L^* (≈52.98–54.27) and high b^* (≈15), typical of cream-colored lime mortars (Table 3). ΔE_{00} values between Nf and the inner cores Nc and Ac (20.77–22.10) (Table 4) are far above commonly adopted thresholds for strong visual differences in heritage contexts, while ΔE_{00} between Nv/Av/Af and the cores (≈3.18–11.33) correspond to small to moderate, yet clearly perceptible shifts. The near-identical color of Nc and Ac (ΔE_{00} = 1.34) confirms that both cores can serve as internal chromatic references for the original appearance of the 2008–2010 mortar.

Taken together, the multi-analytical dataset reconstructs an alteration pathway in which a young restoration mortar has already evolved towards a dark, gypsum- and particulate-laden surface state (Nf), under the influence of urban pollution and microclimatic exposure on the buttress, while verso and core zones preserve a carbonate-dominated, chromatically stable substrate. This combination of rapid surface alteration and preserved inner mortar is consistent with other urban case studies where lime-based repairs act as sensitive recorders of local air quality [60].

4.6.2. Implications for Long-Term Performance Under Urban Stress

The observation that mortars applied only one to two decades ago already support advanced black crusts on the exposed Nf face has direct implications for the expected durability of lime-based repairs on the Golia enclosure wall and, more broadly, in polluted historic centers. Even when compositionally compatible with historic masonry, such mortars can undergo significant surface transformation over relatively short timescales when subjected to persistent SO_x/NO_x, particulate matter and restricted natural washing.

Three groups of long-term risks emerge from the integrated interpretation:

(1) Hydric behavior and salt cycling.

The combined effects of gypsum precipitation, particulate clogging, and partial pore sealing on Nf are likely to reduce surface permeability and promote shallow water retention, thereby enhancing freeze–thaw stress and cyclic dissolution–crystallization of salts. This interpretation is supported by the strong sulfate/gypsum FTIR bands on Nf (Table 6; e.g., ~3400–3450, ~1120–1150, and ~670 cm^{-1}), together with the elevated sulfur signal measured by pXRF (Table 1). In contrast, on Nv and Av, the FTIR spectra are dominated by carbonate

signatures and show only minimal sulfate-related features (Table 6), suggesting that sulfate phases are not abundant at the analyzed surface layer. Nevertheless, S remains detectable on Nv/Av by pXRF and EDX (Tables 1 and 2), which may indicate low-level sulfate occurrence (e.g., finely dispersed phases, early-stage sulfation, or subsurface accumulation below the FTIR effective sampling depth). Under fluctuating relative humidity, such conditions can still favor episodic dissolution and re-precipitation within connected pore pathways, with potential for sub-florescence-related damage if transport pathways evolve over time [61–63].

(2) Mechanical decoupling and scaling.

SEM observations highlight a pronounced microstructural and textural contrast between the altered outer layer and the underlying lime mortar matrix, particularly on the Nf surface (Figure 2). The outer surface exhibits a heterogeneous, particulate-rich morphology, while the substrate appears comparatively mortar-like, implying a potential mismatch in porosity, stiffness, and hygric response across the interface. Such contrasts are known to favor stress concentration under wet–dry and salt-cycling conditions, increasing susceptibility to microcracking and eventual flaking/scaling, especially along edges and corners. Comparable gypsum–carbonaceous crust systems have been reported to detach in scales, exposing fresh substrate to renewed pollutant input and repeating the alteration cycle [64–66].

(3) Pollutant accumulation and bioreceptivity.

Although pXRF indicates no substantial enrichment in toxic heavy metals (e.g., Pb and Zn) (Table 1), the investigated surfaces—particularly Nf—show a particulate-rich altered layer in SEM (Figures 2–5) and aliphatic C–H bands at ~2920 and ~2850 cm^{-1} consistent with carbonaceous/soot-like deposits (FTIR; Table 6). In addition, low-level P by pXRF/EDX (Tables 1 and 2) may be interpreted as a proxy for nutrient. Together, these features suggest that the altered surface can function as a pollutant- and nutrient-retaining interface, which may become increasingly bioreceptive over time. In a broader perspective, the evolution of contamination/patina-like surface layers has been discussed as being driven by coupled pedological, chemical, and microbiological processes [58], while established biological colonization is known to enhance moisture retention, promote local acidification, and contribute to granular disintegration of carbonate-based mortars and stones [55,67,68].

In this context, the inner cores Nc and Ac are not only material references but also conservation benchmarks. Their colorimetric field defines the acceptable chromatic range for the restoration mortar. Future cleaning or partial crust removal should ideally reduce ΔE_{00} between exposed surfaces and Nc/Ac to within the range of small to moderate color differences ($\approx 3 \div 5$ units), as recommended in color-based assessments of stone and mortar treatments [69]. The large present-day ΔE_{00} between Nf and the cores indicates that the current crust state is visually incompatible with the original mortar and justifies targeted intervention.

Moreover, the spatially resolved information suggests a zoning strategy for conservation on the buttress:

- The heavily altered, chromatically shifted Nf surface should be prioritized for cleaning tests, gentle gypsum reduction and monitoring;
- Af, which displays smaller chromatic deviations and more limited microstructural overprinting, may be managed with more conservative or less frequent interventions, focusing on preventive measures (runoff management, reduced splash, mitigation of local pollutant sources) rather than aggressive cleaning.

By combining pXRF, SEM-EDX, FTIR, XRD, OM and colorimetry in repeated campaigns, the Golia mortars could be monitored as a time-resolved recorder of the local urban microclimate, providing feedback both on conservation treatments and on broader environmental changes affecting the monument.

4.6.3. Methodological Constraints and Perspectives for Multi-Analytical Monitoring

The present study also highlights several technical and methodological limitations that need to be considered when interpreting multi-analytical datasets from stone and mortar samples.

Portable XRF, although rapid and non-invasive, is constrained by relatively large spot sizes, heterogeneous grain-scale compositions and reduced sensitivity to light elements (especially P and S) near the detection limit. The very low concentrations of some elements must therefore be treated as semi-quantitative, and subtle enrichments require cross-validation with micro-analytical data. In addition, only a limited number of pXRF spots could be acquired on the small mortar fragments, which restricts the statistical robustness of compositional gradients along the joint.

SEM–EDX and OM provide high-resolution insights into micro textures and phase distributions but rely on destructive sampling and examine only small areas, which may not fully capture the heterogeneity of crusts and mortars. Preparation steps can also bias the representation of highly porous or soluble phases. FTIR and XRD, while powerful for phase identification, are sensitive to issues such as orientation, peak overlap and detection limits for amorphous or nanocrystalline components (e.g., soot, amorphous silica), which may play important roles in crust development but remain under-represented in bulk spectra.

Colorimetry is a robust bridge between analytical signals and visual perception, yet conventional contact instruments provide only point measurements that may miss small-scale mottling and patterning characteristic of black crusts. Variations in illumination, surface roughness and instrument geometry can further complicate inter-comparisons. Recent advances in calibrated imaging and camera-based color mapping on stone and mortars suggest promising avenues to complement spot-based CIE Lab measurements with areal information.

Despite these constraints, the Golia case study demonstrates that a carefully integrated interpretation of pXRF, SEM–EDX, FTIR, XRD, OM and CIE Lab color data can yield a realistic and nuanced alteration model for a young restoration mortar subjected to urban stress. In this model, the 2008–2010 joint mortar on the buttress behaves both as a vulnerable geomaterial—already showing advanced surface alteration—and as an environmental archive. Future work could extend this approach by:

- increasing the density of non-invasive measurements along vertical and horizontal profiles on the wall;
- coupling material data with in situ atmospheric monitoring;
- and integrating additional techniques (e.g., Raman spectroscopy, micro-XRD, hyperspectral imaging) to refine the characterization of crust components and their temporal evolution.

5. Conclusions

The multi-technique investigation of the west enclosure buttress at Golia Monastery has shown that restoration mortars applied only one to two decades ago already exhibit a marked gradient of pollution-driven alteration between exposed, protected and inner-core domains. The combined pXRF, SEM–EDX, FTIR, XRD, OM and CIE Lab data consistently indicate that the outer millimeters of the joints have evolved towards gypsum- and

particulate-bearing black crusts on the most exposed face (Nf), while verso and core zones still preserve the microstructural and chromatic features of a relatively unaltered mortar.

Geochemical and mineralogical signatures reveal that alteration is clearly directional with respect to the geometry of the wall and buttress and to the orientation of the investigated joint towards the traffic corridor on George Enescu Street. Sulfur enrichment and elevated S/Ca ratios at the exposed face, together with gypsum-related FTIR and XRD signals and quartz-rich dust accumulations, point to a surface-directed sulfation and soiling process, externally fed by urban aerosols. At the same time, enhanced hydrated sulfates in verso zones indicate partial inward redistribution and recrystallization of calcium sulfate, so that external particulate deposition and internal sulfate storage form a coupled alteration system on the Golia mortars.

The directional character of these changes is further controlled by the local microclimate and hydric regime. The buttress is subjected to a persistent daily "atmospheric wake" generated by road traffic, which favors the impingement of polluted air masses on the wall, and to repeated splashing of meteoric and road wash water towards the joints during wet periods. Under the climatic conditions typical of Iași and the north-eastern region of Romania—characterized by alternations between prolonged drought and short episodes of intense rainfall—these processes jointly enhance the frequency of wetting–drying cycles, promote shallow gypsum precipitation and particulate clogging at pore mouths and contribute to the rapid visual darkening quantified by the colorimetric data.

The exposed black-crusted face (Nf) has reached a chromatic state that is clearly incompatible with the inner-core references (Nc, Ac), indicating the need for targeted cleaning tests and monitoring if the visual integrity of the buttress of the western enclosure wall is to be maintained.

Methodologically, the case study demonstrates that an integrated protocol combining portable XRF, micro-analytical techniques (SEM–EDX, FTIR, XRD), optical microscopy and CIE Lab colorimetry can reconstruct, with relatively limited sampling effort, the early stages of black crust evolution on historic mortars under urban stress.

Supplementary Materials: The following supporting information can be downloaded at: https://www.mdpi.com/article/10.3390/app16042080/s1, Table S1: Raw pXRF dataset (spot-level replicates) and descriptive statistics (mean ± SD) for the investigated mortar/crust surfaces, including derived ratio: S/Ca, SiO_2/Ca, and SiO_2/Al_2O_3; Figure S1: Raw FTIR spectra of the investigated mortar surfaces (Nf, Nv, Af and Av); Table S2: Raw CIE *L*a*b** colorimetric spot measurements and descriptive statistics (surface mean and SD) for the investigated mortar surfaces (Nf, Nv, Af, Av, Nc, Ac).

Author Contributions: Conceptualization, V.P., I.S. and S.G. (Silviu Gurlui); methodology, V.P. and I.S.; software, V.P.; formal analysis, V.P.; investigation, V.P. (fieldwork and sampling, pXRF, OM, colorimetry), S.G. (Silvia Garofalide) (fieldwork and sampling), V.V. (SEM–EDX, FTIR, OM, colorimetry), O.C. (XRD), I.-A.D. (XRD), and B.A. (historical documentation); data curation, V.P.; writing—original draft preparation, V.P.; writing—review and editing, V.P. and I.S.; visualization, V.P., I.S. and S.G. (Silviu Gurlui); supervision, I.S. All authors have read and agreed to the published version of the manuscript.

Funding: Grant agreement MySMIS No. 127324, under Operational Program Competitiveness 2014–2020, Axis 1, under POC/448/1/1.

Institutional Review Board Statement: Not applicable.

Informed Consent Statement: Not applicable.

Data Availability Statement: The original contributions presented in this study are included in the article. Further inquiries can be directed to the corresponding authors.

Acknowledgments: This work was supported by infrastructure from the Operational Program Competitiveness 2014–2020, Axis 1, under POC/448/1/1 Research infrastructure projects for public R&D institutions/Sections F 2018, through the Research Center with Integrated Techniques for Atmospheric Aerosol Investigation in Romania (RECENT AIR) project, under grant agreement MySMIS no. 127324. The authors gratefully acknowledge Georgiana Bulai (Alexandru Ioan Cuza University of Iasi) for her technical assistance and support during the XRD laboratory investigations.

Conflicts of Interest: The authors declare no conflicts of interest.

Abbreviations

The following abbreviations are used in this manuscript:

pXRF	Portable X-ray fluorescence
SEM-EDX	Scanning electron microscopy with energy-dispersive X-ray analysis
FTIR	Fourier Transform Infrared Spectroscopy
XRD	X-ray diffraction
CIE	Commission Internationale de l'Éclairage
Lab	three-dimensional ($L^*a^*b^*$) color space defined by the CIE
OM	optical microscopy

References

1. Pozo-Antonio, J.S.; Cardell, C.; Comite, V.; Fermo, P. Characterization of Black Crusts Developed on Historic Stones with Diverse Mineralogy under Different Air Quality Environments. *Environ. Sci. Pollut. Res.* **2022**, *29*, 29438–29454. [CrossRef]
2. Marszałek, M.; Dudek, K.; Gaweł, A. Black Crust from Historic Buildings as a Natural Indicator of Urban Environmental Contamination: A Case Study of the Lipowiec Castle in Southern Poland. *Sustainability* **2024**, *16*, 3816. [CrossRef]
3. Wilhelm, K.; Longman, J.; Standish, C.D.; De Kock, T. The Historic Built Environment as a Long-Term Geochemical Archive: Telling the Time on the Urban "Pollution Clock". *Environ. Sci. Technol.* **2023**, *57*, 12362–12375. [CrossRef]
4. Bacci, M. Black rusts as pollution indicators. In *The Effects of Air Pollution on the Built Environment*; Brimblecombe, P., Ed.; Air Pollution Reviews; Imperial College Press: London, UK, 1991; Volume 2, pp. 225–243.
5. Briones, C.C.; Pinilla, S.M.; Moliní, D.V.; Fernández-Balbuena, A.A. Colorimetry to Assess the Visual Impact of Dust Deposition on Mosaics at Sheltered Archaeological Sites. *Herit. Sci.* **2021**, *9*, 40. [CrossRef]
6. Postolachi, C.; Cocean, A.; Garofalide, S.; Munteanu, B.S.; Cocean, G.; Cimpoesu, N.; Pelin, V.; Cocean, I.; Gurlui, S. Urban Exotic Pollution: The Harmful Environmental Footprint for Health and Historical Architecture. *Int. J. Environ. Res. Public Health* **2023**, *20*, 4715. [CrossRef]
7. Moropoulou, A.; Bakolas, A.; Bisbikou, K. Physico-chemical Adhesion and Cohesion Bonds in Joint Mortars Imparting Durability to the Historic Structures. *Constr. Build. Mater.* **2000**, *14*, 35–46. [CrossRef]
8. Caroselli, M.; Ruffolo, S.A.; Piqué, F. Mortars and Plasters—How to Manage Their Conservation. *Archaeol. Anthropol. Sci.* **2021**, *13*, 188. [CrossRef]
9. Aggelakopoulou, E.; Bakolas, A.; Moropoulou, A. Evaluation of Mortar Mix Designs for the Conservation of the Acropolis Monuments. *J. Cult. Herit.* **2022**, *55*, 300–308. [CrossRef]
10. Comite, V.; Pozo-Antonio, J.S.; Cardell, C.; Randazzo, L.; La Russa, M.F.; Fermo, P. A Multi-Analytical Approach for the Characterization of Black Crusts on the Façade of an Historical Cathedral. *Microchem. J.* **2020**, *158*, 105121. [CrossRef]
11. Macchia, A.; Cerafogli, E.; Rivaroli, L.; Colasanti, I.A.; Aureli, H.; Biribicchi, C.; Brunori, V. Marble Chromatic Alteration Study Using Non-Invasive Analytical Techniques and Evaluation of the Most Suitable Cleaning Treatment: The Case of a Bust Representing Queen Margherita di Savoia at the U.S. Embassy in Rome. *Analytica* **2022**, *3*, 406–429. [CrossRef]
12. Lorusso, S.; Natali, A.; Matteucci, C. Colorimetry Applied to the Field of Cultural Heritage: Examples of Study Cases. *Conserv. Sci. Cult. Herit.* **2007**, *7*, 187–220. [CrossRef]
13. Pelin, V.; Ratoi, B.; Apavaloaei, B.; Vasilache, V.; Sandu, I.; Branzila, M. Conservation state assessment of the Golia Monastery enclosure wall. In *Monument Future: Decay and Conservation of Stone, Proceedings of the 14th International Congress on the Deterioration and Conservation of Stone (STONE 2020)*; Siegesmund, S., Middendorf, B., Eds.; Mitteldeutscher Verlag: Halle (Saale), Germany, 2020; pp. 1089–1096.
14. Pelin, V.; Garofalide, S.; Sandu, I.; Apavaloaei, B.; Gurlui, S. Black Crust versus Substrate on Historic Stone: A Brief pXR Study at Golia Monastery (Iași, Romania). *Int. J. Conserv. Sci.* **2025**, *16*, 1979–1992. [CrossRef]
15. Sandu, I. Modern Aspects Regarding the Conservation of Cultural Heritage Artifacts. *Int. J. Conserv. Sci.* **2022**, *13*, 1187–1208. [CrossRef]

16. Sandu, I.; Sandu, I.C.A. New Interdisciplinary Aspects on Science for Conservation of Cultural heritage (II). *Egypt. J. Archaeol. Restor. Stud.* **2013**, *3*, 73–83. [CrossRef]
17. Sandu, I.C.A.; Spiridon, P.; Sandu, I. Current Studies and Approaches in the Field of Cultural Heritage Conservation Science: Harmonizing the Terminology in an Interdisciplinary Context. *Int. J. Conserv. Sci.* **2016**, *7*, 591–606.
18. Sandu, I. New Materials and Advanced Procedures of Conservation Ancient Artifacts. *Appl. Sci.* **2023**, *13*, 8387. [CrossRef]
19. Sandu, I.; Deak, G.; Ding, Y.; Ivashko, Y.; Sandu, A.V.; Moncea, A.; Sandu, I.G. Materials for Finishing of Ancient Monuments and Process of Obtaining and Applying. *Int. J. Conserv. Sci.* **2021**, *12*, 1249–1258.
20. Available online: https://www.crystalimpact.de/match/ (accessed on 20 January 2026).
21. Mokrzycki, W.S.; Tatol, M. Color difference Delta E—A survey. *Mach. Graph. Vis.* **2011**, *20*, 383–411. Available online: https://www.researchgate.net/publication/236023905_Color_difference_Delta_E_-_A_survey (accessed on 7 January 2026).
22. Sharma, G.; Wu, W.C.; Daa, E.N. The CIEDE2000 Color-Difference Formula: Implementation Notes, Supplementary Test Data, and Mathematical Observations. *Color Res. Appl.* **2005**, *30*, 21–30. [CrossRef]
23. Sánchez, J.S.; Romani, J.R.; Mosquera, D.F.; Alves, C.A. Study of origin and composition of coatings in a monument built with granitic rocks, by SEM, XRD, XRF and DTA-TGA. *X-Ray Spectrom.* **2008**, *37*, 346–354. [CrossRef]
24. Sánchez, J.S.; Romaní, J.R.V.; Alves, C. Deposition of particles on gypsum-rich coatings of historic buildings in urban and rural environments. *Constr. Build. Mater.* **2011**, *25*, 813–822. [CrossRef]
25. Morillas, H.; Maguregui, M.; García-Florentino, C.; Carrero, J.A.; Salcedo, I.; Madariaga, J.M. The cauliflower-like black crusts on sandstones: A natural passive sampler to evaluate the surrounding environmental pollution. *Environ. Res.* **2016**, *147*, 218–232. [CrossRef] [PubMed]
26. Shackley, M.S. X-Ray, An Introduction to X-Ray Fluorescence (XRF). Analysis in Archaeology. In *X-Ray Fluorescence Spectro-Metry (XRF) in Geoarchaeology*; Shackley, M.S., Ed.; Springer: New York, NY, USA, 2011; p. 18. [CrossRef]
27. Vilarigues, M.; Redol, P.; Machado, A.; Rodrigues, P.A.; Alves, L.C.; da Silva, R.C. Corrosion of 15th and early 16th century stained glass from the monastery of Batalha studied with external ion beam. *Mater. Charact.* **2011**, *62*, 211–217. [CrossRef]
28. Kumar, G.; Rusin, L.; Nagar, P.K.; Manjul, S.K.; Back, M.; Benedetti, A.; Gurjar, B.R.; Ojha, C.S.P.; Sharma, M.; Balliana, E. Characterization of Red Sandstone and Black Crust to Analyze Air Pollution Impacts on a Cultural Heritage Building: Red Fort, Delhi, India. *Heritage* **2025**, *8*, 236. [CrossRef]
29. Ikuta, D.; Kawame, N.; Banno, S.; Hirajima, T.; Ito, K.; Rakovan, J.F.; Downs, R.T.; Tamada, O. First in situ X-ray identification of coesite and retrograde quartz on a glass thin section of an ultrahigh-pressure metamorphic rock and their crystal structure details. *Am. Mineral.* **2007**, *92*, 57–63. [CrossRef]
30. Sitepu, H.; O'Connor, B.H.; Li, D. Comparative evaluation of the March and generalized spherical harmonic preferred orientation models using X-ray diffraction data for molybdite and calcite powders. *J. Appl. Crystallogr.* **2005**, *38*, 158–167. [CrossRef]
31. Cole, W.F.; Lancucki, C.J. A refinement of the crystal structure of gypsum $CaSO_4 \cdot 2H_2O$. *Acta Crystallogr. Sect. B Struct. Sci.* **1974**, *30*, 921–929. [CrossRef]
32. CIE (Commission Internationale de l'Éclairage). *Official Recommendations on Uniform Color Spaces, Color-Difference Equations and Metric Color Terms*; Supplement No. 2 (1978) to CIE Publication No. 15 (E-1.3.1) (1971); Central Bureau of the CIE: Vienna, Austria, 1976. Available online: https://cie.co.at/publications/colorimetry-part-4-cie-1976-lab-colour-space-0 (accessed on 8 December 2025).
33. Tokarska, M.; Miśkiewicz, P.; Puszkarz, A.K.; Nosal, A. Evaluation of Insulation against Contact Heat, Radiant Heat and Sensory Comfort of Basalt Fabric-Based Composites with Parylene C Coating. *Fibres Text. East. Eur.* **2023**, *31*, 99–108. [CrossRef]
34. Elsen, J. Microscopy of historic mortars—A review. *Cem. Concr. Res.* **2006**, *36*, 1416–1424. [CrossRef]
35. Moropoulou, A.; Bakolas, A.; Bisbikou, K. Investigation of the technology of historic mortars. *J. Cult. Herit.* **2000**, *1*, 45–58. [CrossRef]
36. Gheris, A. New dating approach based on the petrographical, mineralogical and chemical characterization of ancient lime mortar: Case study of the archaeological site of Hippo, Annaba city, Algeria. *Herit. Sci.* **2023**, *11*, 103. [CrossRef]
37. Frahm, E. Protocols, pitfalls, and publishing for pXRF analyses: From "know how" to "best practices". *J. Archaeol. Sci. Rep.* **2024**, *60*, 104831. [CrossRef]
38. Drake, B.L. Appendix A: Element Guide. In *Advances in Portable X-Ray Fluorescence Spectrometry: Instrumentation, Application and Interpretation*; Drake, B.L., MacDonald, B.L., Eds.; Royal Society of Chemistry: Cambridge, UK, 2022. Available online: https://www.rsc.org/suppdata/books/178801/9781788014229/bk9781788014229.pdf (accessed on 8 December 2025). [CrossRef]
39. Dakal, T.C.; Cameotra, S.S. Microbially Induced Deterioration of Architectural Heritages: Routes and Mechanisms Involved. *Environ. Sci. Eur.* **2012**, *24*, 36. [CrossRef]
40. Pozo-Antonio, J.S.; Pereira, M.F.C.; Rocha, C.S.A. Microscopic characterisation of black crusts on different substrates. *Sci. Total Environ.* **2017**, *584*, 291–306. [CrossRef]
41. Toniolo, L.; Zerbi, C.M.; Bugini, R. Black layers on historical architecture. *Environ. Sci. Pollut. Res.* **2009**, *16*, 218–226. [CrossRef]

42. Wang, F.; Fu, Y.C.; Li, D.; Huang, Y.Z.; Wei, S.Y. Study on the mechanism of the black crust formation on the ancient marble sculptures and the effect of pollution in Beijing area. *Heliyon* **2022**, *8*, e10442. [CrossRef]
43. Ruffolo, S.A.; La Russa, M.F.; Rovella, N.; Ricca, M. The Impact of Air Pollution on Stone Materials. *Environments* **2023**, *10*, 119. [CrossRef]
44. Melo, H.P.; Cruz, A.J.; Candeias, A.; Mirão, J.; Cardoso, A.M.; Oliveira, M.J.; Valadas, S. Problems of analysis by FTIR of calcium sulphate–based preparatory layers: The case of a group of 16th-century Portuguese paintings. *Archaeometry* **2014**, *56*, 513–526. [CrossRef]
45. Zeb, B.; Alam, K.; Sorooshian, A.; Blaschke, T.; Ahmad, I.; Shahid, I. On the Morphology and Composition of Particulate Matter in an Urban Environment. *Aerosol Air Qual. Res.* **2018**, *18*, 1431–1447. [CrossRef]
46. El-Sheikh, S.M.; Barhoum, A.; El-Sherbiny, S.; Morsy, F.; El-Midany, A.A.-H.; Rahier, H. Preparation of superhydrophobic nanocalcite crystals using Box–Behnken design. *Arab. J. Chem.* **2019**, *12*, 1479–1486. [CrossRef]
47. Maor, Y.; Toffolo, M.B.; Feldman, Y.; Vardi, J.; Khalaily, H.; Asscher, Y. Dolomite in archaeological plaster: An FTIR study of the plaster floors at Neolithic Motza, Israel. *J. Archaeol. Sci. Rep.* **2023**, *48*, 103862. [CrossRef]
48. Calandra, S.; Cantisani, E.; Salvadori, B.; Barone, S.; Liccioli, L.; Fedi, M.; Garzonio, C.A. Evaluation of ATR-FTIR spectroscopy for distinguish anthropogenic and geogenic calcite. *J. Phys. Conf. Ser. IOP Publ.* **2022**, *2204*, 012048. [CrossRef]
49. Jordán, M.M.; Jordá, J.; Pardo, F.; Montero, M.A. Mineralogical Analysis of Historical Mortars by FTIR. *Materials* **2019**, *12*, 55. [CrossRef] [PubMed]
50. Sabbioni, C. Mechanisms of Air Pollution Damage to Stone. In *The Effects of Air Pollution on the Built Environment*; Brimblecombe, P., Ed.; Air Pollution Reviews; Imperial College Press: London, UK, 2003; Volume 2, pp. 63–106.
51. Yates, T. Mechanisms of Air Pollution Damage to Brick, Concrete and Mortar. In *The Effects of Air Pollutionon the Built Environment*; Brimblecombe, P., Ed.; Air Pollution Reviews; Imperial College Press: London, UK, 2003; Volume 2, pp. 107–132.
52. Grossi, C.M.; Brimblecombe, P.; Esbert, R.M.; Alonso, F.J. Color changes in architectural limestones from pollution and cleaning. *Color Res. Appl.* **2007**, *32*, 320–331. [CrossRef]
53. Perez-Monserrat, E.M.; Varas-Muriel, M.J.; De Buergo, M.A.; Fort, R. Black Layers of Decay and Color Patterns on Heritage Limestone as Markers of Environmental Change. *Geosciences* **2016**, *6*, 4. [CrossRef]
54. Macchia, A.; Brunori, V.; Rivaroli, L.; Coronas, P.; Balzani, C.; Rovella, N. Colorimetric Monitoring of Palazzo Margherita, US Embassy in Rome. *Int. J. Conserv. Sci.* **2020**, *11*, 261–270.
55. Berti, L.; Arfelli, F.; Villa, F.; Cappitelli, F.; Gulotta, D.; Ciacci, L.; Bernardi, E.; Vassura, I.; Passarini, F.; Napoli, S.; et al. LCA as a Complementary Tool for the Evaluation of Biocolonization Management: The Case of Palazzo Rocca Costaguta. *Heritage* **2024**, *7*, 6871–6890. [CrossRef]
56. Ratoi, B.; Pelin, V.; Sandu, I.; Branzila, M.; Sandu, I.G. Hidden Message in Stone Masonry of Galata Monastery—Iași City, Romania. *Int. J. Conserv. Sci.* **2018**, *9*, 151–164.
57. Sandu, I.; Lupascu, E.; Sandu, I.C.A.; Ivashko, Y. Artefactometrical Assessment of Works of Art by Summing the Impact Grids of Altmetric Quantification. *Egypt. J. Archaeol. Restor. Stud.* **2023**, *13*, 185–195. [CrossRef]
58. Sanjurjo-Sánchez, J.; Alves, C.; Freire-Lista, D.M. Biomineral deposits and coatings on stone monuments as biodeterioration fingerprints. *Sci. Total Environ.* **2024**, *912*, 168846. [CrossRef] [PubMed]
59. Bergomi, A.; Comite, V.; Borelli, M.; Lombardi, C.A.; Festa, E.; Oujja, M.; Castillejo, M.; Maestro-Guijarro, L.; Carmona-Quiroga, P.M.; Crespo, A.; et al. Integrated Comprehensive Characterization of Black Crusts from Milan's Monumental Cemetery: A Synergistic Approach Combining Conventional and Unconventional Analytical Techniques. *Heritage* **2025**, *8*, 506. [CrossRef]
60. Grossi, C.M.; Brimblecombe, P. Effect of long-term changes in air pollution and climate on the decay and blackening of European stone buildings. In *Building Stone Decay from Diagnosis to Conservation*; Bernard, J., Přikryl, R., Smith, B.J., Eds.; Special Publications; Geological Society Publishing House/Geological Society London: Bath, UK, 2007; Volume 271, pp. 117–130. Available online: https://www.lyellcollection.org/toc/sp/271/1 (accessed on 8 December 2025). [CrossRef]
61. Marszałek, M.; Dudek, K.; Gaweł, A. Cement Render and Mortar and Their Damages Due to Salt Crystallization in the Holy Trinity Church, Dominicans Monastery in Cracow, Poland. *Minerals* **2020**, *10*, 641. [CrossRef]
62. Ahmad, A.G.; Rahman, H.F.A. Treatment of salt attack and rising damp in heritage buildings in Penang, Malaysia. *J. Constr. Dev. Ctries* **2010**, *15*, 93–113. Available online: http://web.usm.my/jcdc/vol15_1_2010.html (accessed on 8 December 2025).
63. Todorović, J.; Janssen, H. The impact of salt pore clogging on the hygric properties of bricks. *Constr. Build. Mater.* **2018**, *164*, 850–863. [CrossRef]
64. Török, Á. Gypsum-induced Decay on Limestone Buildings in the Urban Environment of Budapest/Gipsinduzierter Zerfall des Kalksteins in städtischer Atmosphäre in Budapest. *Restor. Build. Monum.* **2005**, *11*, 71–78. [CrossRef]
65. van Hees, R.P.J.; Binda, L.; Papayianni, I.; Toumbakari, E. Damage Analysis as a Step Towards Compatible Repair Mortars. In *Characterisation of Old Mortars with Respect to Their Repair*; Report 28; Groot, C., Ashall, G.J., Hughes, J., Eds.; RILEM Publications SARL: Bagneux, France, 2004; pp. 105–124. [CrossRef]

66. La Russa, M.F.; Ruffolo, S.A. Mortars and plasters—How to characterize mortar and plaster degradation. *Archaeol. Anthropol. Sci.* **2021**, *13*, 165. [CrossRef]
67. Liu, X.B.; Koestler, R.J.; Warscheid, T.; Katayama, Y.; Gu, J.D. Microbial Deterioration and Sustainable Conservation of Stone Monuments and Buildings. *Nat. Sustain.* **2020**, *3*, 991–1004. [CrossRef]
68. Warscheid, T.; Braams, J. Biodeterioration of stone: A review. *Int. Biodeterior. Biodegrad.* **2000**, *46*, 343–368. [CrossRef]
69. Wang, W.; Wang, S.; Liu, Q.; Wang, X.F.; Zhu, J.F.; Luo, H.J.; Ji, S.D. Study on the efficacy of amorphous calcium carbonate as a consolidant for calcareous matrix. *Herit. Sci.* **2022**, *10*, 165. [CrossRef]

Disclaimer/Publisher's Note: The statements, opinions and data contained in all publications are solely those of the individual author(s) and contributor(s) and not of MDPI and/or the editor(s). MDPI and/or the editor(s) disclaim responsibility for any injury to people or property resulting from any ideas, methods, instructions or products referred to in the content.